



HAL
open science

Maximum glacier extent of the Penultimate Glacial Cycle in the Upper Garonne Basin (Pyrenees): new chronological evidence

Marcelo Fernandes, Marc Oliva, Gonçalo Vieira, David Palacios, José María Fernández-Fernández, Magali Delmas, Julia García-Oteyza, Irene Schimmelpfennig, Josep Ventura, Georges Aumaître, et al.

► To cite this version:

Marcelo Fernandes, Marc Oliva, Gonçalo Vieira, David Palacios, José María Fernández-Fernández, et al.. Maximum glacier extent of the Penultimate Glacial Cycle in the Upper Garonne Basin (Pyrenees): new chronological evidence. *Environmental Earth Sciences*, 2021, 80 (24), pp.796. 10.1007/s12665-021-10022-z . hal-03450430

HAL Id: hal-03450430

<https://hal.science/hal-03450430>

Submitted on 24 Aug 2023

HAL is a multi-disciplinary open access archive for the deposit and dissemination of scientific research documents, whether they are published or not. The documents may come from teaching and research institutions in France or abroad, or from public or private research centers.

L'archive ouverte pluridisciplinaire **HAL**, est destinée au dépôt et à la diffusion de documents scientifiques de niveau recherche, publiés ou non, émanant des établissements d'enseignement et de recherche français ou étrangers, des laboratoires publics ou privés.

[Click here to view linked References](#)

Maximum glacier extent of the Penultimate Glacial Cycle in the Upper Garonne Basin (Pyrenees): new chronological evidence

M. Fernandes¹, M. Oliva², G. Vieira¹, D. Palacios³, J.M. Fernández-Fernández¹, M. Delmas⁴, J. García-Oteyza², I. Schimmelpfennig⁵, J. Ventura² & ASTER Team^{5,6}

¹ Centre for Geographical Studies, Instituto de Geografia e Ordenamento do Território, Universidade de Lisboa, Lisbon, Portugal

² Department of Geography, Universitat de Barcelona, Barcelona, Catalonia, Spain

³ Department of Geography, Universidad Complutense de Madrid, Madrid, Spain

⁴ HNHP UMR 7194, Université de Perpignan Via Domitia, Perpignan, France

⁵ Aix-Marseille Université, CNRS, IRD, INRAE, Coll. France, UM 34 CEREGE, Aix-en-Provence, France

⁶ Consortium: Georges Aumaître, Karim Keddadouche

Corresponding author

Marcelo Fernandes, marcelo.fernandes@live.com

Centre for Geographical Studies – IGOT, University of Lisbon

Rua Branca Edmée Marques, 1600-276 Lisbon, Portugal

Tel: +351962277913

Abstract

1 The Upper Garonne Basin included the longest glacier in the Pyrenees during the Late Pleistocene. During
2 major glacial advances, the Garonne palaeoglacier flowed northwards along ~80 km from peaks of the axial
3 Pyrenees exceeding 2,800-3,000 m until the foreland of this mountain range at the Loures-Barousse-Barbazan
4 basin (LBBb), at 420-440 m. Here, the palaeoglacier formed a terminal moraine complex that is examined in
5 this work. Based on geomorphological observations and a 12-sample dataset of ¹⁰Be Cosmic-Ray Exposure
6 (CRE) ages, the timing of the maximum glacial extent was constrained as well as the onset of the deglaciation
7 from the end of the Last Glacial Cycle (LGC). Chronological data shows evidence that the external moraines
8 in this basin were abandoned by the ice at the end of the Penultimate Glacial Cycle (PGC) and the onset of the
9 Eemian Interglacial, at ~129 ka. No evidence of subsequent glacial advances or standstills occurred during the
10 LGC in this basin were found, as the few existing datable boulders provided in the internal moraine showed
11 inconsistent ages, thus probably being affected by post-glacial processes. The terminal basin was already
12 deglaciated during the global Last Glacial Maximum at 24-21 ka, as revealed by exposure ages of polished
13 surfaces at the confluence of the Garonne-La Pique valleys, 13 km south of the entrance of the LBBb. This
14 study introduces the first CRE ages in the Pyrenees for the glacial advance occurred during the PGC and
15 provides also new evidence that glaciers had already significantly shrunk during the LGM.
16
17

18
19 **Key words:** Central Pyrenees, Upper Garonne Basin, Penultimate Glacial Cycle, Cosmic-Ray Exposure
20 dating, moraines, polished bedrock.
21
22
23
24
25
26
27
28
29
30
31
32
33
34
35
36
37
38
39
40
41
42
43
44
45
46
47
48
49
50
51
52
53
54
55
56
57
58
59
60
61
62
63
64
65

Declarations

Funding: This research was financially supported by the Research Group ANTALP (Antarctic, Arctic, Alpine Environments; 2017-SGR-1102) funded by the Government of Catalonia and the Centro de Estudos Geográficos/IGOT - University of Lisbon (FCT I.P. UIDB/00295/2020 and UIDP/00295/2020). The study topics complement those of the project PALEOGREEN (CTM2017-87976-P) funded by the Spanish Ministry of Economy and Competitiveness and the project NUNANTAR funded by the Fundação para a Ciência e Tecnologia of Portugal (02/SAICT/2017 - 32002). Marcelo Fernandes currently holds a PhD fellowship of the Fundação para a Ciência e Tecnologia of Portugal (FCT - SFRH/139569/2018); Marc Oliva is supported by the Ramón y Cajal Program (RYC-2015-17597) and José M. Fernández-Fernández is supported by a postdoctoral grant within the NUNANTAR project. ¹⁰Be measurements were performed at the ASTER AMS national facility (CEREGE, Aix-en-Provence), which is supported by the INSU/CNRS and the ANR through the “Projets thématiques d'excellence” program for the “Equipements d'excellence” ASTER-CEREGE action and IRD. This work is also framed within the College on Polar and Extreme Environments (Polar2E) of the University of Lisbon.

Competing interests: The authors declare that they have no known competing financial interests or personal relationships that could have appeared to influence the work reported in this paper.

Availability of data and material: The data presented in this article are openly available in this website: <http://alpine.ice-d.org/>

Code availability: The geomorphological map was developed using ArcGIS 10.7.1 (ESRI) software based on the UTM projection and the ETRS89 zone 31N coordinate system. The layouts were improved with the Inkscape 1.0 software.

Authors' contributions:

1. Marcelo Fernandes. Laboratory tasks (sample processing), collection and handling of aerial photo imagery, geomorphological mapping and writing of a first draft of the manuscript.
2. Marc Oliva. Coordination of the research, funding acquisition, field work, geomorphological analysis, sampling, data processing and contributing to the writing and final revision of the manuscript.
3. Gonçalo Vieira. Geomorphological analysis, discussion of results, contribution to the writing and final revision of the manuscript.
4. David Palacios. Fieldwork, geomorphological analysis, discussion of the results, and contribution to the writing and final revision of the manuscript.
5. José M. Fernández-Fernández. Laboratory tasks (sample processing, exposure age calculations), contribution to the writing and final revision of the manuscript.
6. Magali Delmas. Geomorphological analysis, discussion of results, contribution to the final revision of the manuscript.
7. Julia García-Oteyza. Laboratory tasks (sample processing, exposure age calculations), contribution to the writing and final revision of the manuscript.
8. Irene Schimmelpfennig. Supervision of the whole process of the sample processing and interpretation of the results, contribution to the writing and final revision of the manuscript.
9. Josep Ventura. Fieldwork, geomorphological analysis, discussion of results, contribution to the writing and final revision.
10. ASTER Team. Supervision of the AMS measurements of the ³⁶Cl samples.

Ethics approval: 'Not applicable'

Consent to participate: 'Not applicable'

Consent for publication: 'Not applicable'

1. Introduction

High and middle mountain landscapes in mid-latitude ranges have been mostly shaped by glaciers during Pleistocene glacial cycles. Large valleys, glacial cirques, truncated spurs, hanging valleys (large-scale erosional landforms) and till or moraines (accumulation landforms) constitute the legacy of the past glaciations in the highest massifs (Benn and Evans 2010). Such invaluable glacial footprints can provide a better understanding of past environmental and climatic changes (Pearce et al. 2017).

The widespread glacial features existing in mid-latitude and Mediterranean mountains have been increasingly used to reconstruct the timing, magnitude and extent of the glacial oscillations during past glacial cycles (Ehlers et al. 2011; Adamson et al. 2013). The study of glacial advances and retreats has mostly focused on the Late Pleistocene (or Last Glacial Cycle, LGC), from the end of the Eemian Interglacial (129-114 ka) to the Holocene (11.7 ka to present; Dahl-Jensen et al. 2013; Rasmussen et al. 2014). Glacial studies have resulted in an increase in the number and accuracy of regional and global palaeoclimate records, which generally show a good coupling between cold phases and glacial advances (Bernal-Wormull et al. 2021; González-Sampériz et al. 2006; Morellón et al. 2009; Lisiecki and Raymo 2005, Rasmussen et al. 2014). In the Pyrenees, where this research focuses on, currently available data indicate that the most extensive Pyrenean glaciation of the Late Pleistocene occurred prior to the global Last Glacial Maximum (gLGM: 26-19 ka; Clark et al. 2009). This outermost stadial position (local Last Glacial Maximum; ILGM) was reached not just once, but several times between MIS 5b (or MIS 4) and MIS 3 (Fig. 1a; Mardones and Jalut 1983; Andrieu et al. 1988; García-Ruiz et al. 2003, 2013; Lewis et al. 2009; Pallàs et al. 2010; Delmas et al. 2011; Turu et al. 2016; Sancho et al. 2018; Tomkins et al. 2018; Synthesis in Delmas et al. 2021a). The dimensions of Pyrenean glaciers at the time of the gLGM are well established in the eastern part of the range, where ^{10}Be , ^{36}Cl and Schmidt hammer exposure ages have been obtained from boulders embedded in moraines and from ice-scoured rock steps protruding from valley floors (Fig. 1a; Pallàs et al. 2006, 2010; Delmas et al. 2008; Palacios et al. 2015a; Andrés et al. 2018; Tomkins et al. 2018; Synthesis in Delmas et al. 2021b). By contrast, in the westernmost valleys of the Pyrenees, glacier dimensions at the time of the gLGM remain imprecisely defined because age constraints are mainly provided by glaciolacustrine deposits (Andrieu 1987 1991; Andrieu et al. 1988; Jalut et al. 1988; Montserrat-Martí 1992; Reille and Andrieu 1995; García-Ruiz et al. 2003; Synthesis in Delmas et al. 2021b). Besides, other periods of glacial advance and retreat during Termination I are also well-known for northern and southern valleys (Copons and Bordonau 1996; Pallàs et al. 2006, 2010; Delmas et al. 2008, 2011; Palacios et al. 2015a, 2015b, 2017; Crest et al. 2017; Andrés et al. 2018; Tomkins et al. 2018; Fernandes et al. 2021; Oliva et al. 2021; Reixach et al. 2021).

Middle Pleistocene glaciations in the Pyrenees remain poorly documented (Fig. 1a; Synthesis in Delmas et al. 2021a). Most chronological evidence concerning ice-margin fluctuations prior to the Late Pleistocene glacial cycle is known thanks to U-Th ages in cave systems of limestone massifs (Bakalowicz et al. 1984; Quinif and Maire 1998; Sorriaux et al. 2016) and TCN profiles, OSL, ESR ages on glaciofluvial terraces (Turu and Peña 2006; Turu et al. 2007; Lewis et al. 2009; García-Ruiz et al. 2013; Delmas et al. 2015, 2018). Only one ^{10}Be exposure age at 133.9 ± 5.3 ka has been obtained from an erratic boulder abandoned by the Ariège Glacier at Caraybat (Delmas et al. 2011). This age also validates the post-depositional weathering criteria to differentiate those glacial deposits from older than MIS 5e and MIS 5d-MIS 2 (Gourinard 1971; Hubschman 1975, 1984; Héту and Gangloff 1989; Gangloff et al. 1991; Héту et al. 1992; Calvet 1996).

During the last two glacial cycles, the Central Pyrenees included large ice fields from where composite glaciers flowed downvalley for several tens of km forming piedmont features in the northern foreland and valley glaciers in the southern slope (Fig. 1B). The Upper Garonne Valley hosted the longest Pyrenean palaeoglacier, with an ice tongue following northwards for ~80 km down to the Loures-Barousse-Barbazan basin (LBBb) and reaching an elevation of 420-440 m a.s.l. (Andrieu 1991; Calvet et al. 2011). Previous studies based on the degree of soil development and on the state of the weathering of granite cobbles and boulders contained within the glacial sediments revealed the presence of two main morainic complexes in that area: (i) the outermost one surrounding the external northern fringe of the basin is supposed to correspond to the Penultimate Glacial Cycle (PGC; i.e. ~192-135 ka; Obrochta et al. 2015); while (ii) the moraine ridges distributed across the internal part of the basin were associated with the LGC (Hubschman 1975, 1984; Stange et al. 2014). Radiocarbon ages obtained within the Barbazan glaciolacustrine sequence confirmed this relative chronology (Andrieu 1991; Andrieu et al. 1988), even if these ages are controversial, as potential problems associated with hard water effect in the carbon content were raised by other authors (Pallàs et al. 2006).

1 In order to shed light on the glacial chronology of the largest expansion of the PGC and LGC glaciers in the
2 northern slope of the Pyrenees, new Cosmic-Ray Exposure (CRE) ages are presented from glacial landforms
3 distributed across the LBBb aiming to answer the following questions:

- 4 - When did Pleistocene glaciers reach their maximum extent in the Central Pyrenees?
- 5 - Are there glacial remnants from the PGC as previously inferred from post-depositional weathering
6 intensity criteria?
- 7 - When did glaciers start retreating and abandoned the Loures-Barousse-Barbazan terminal basin
8 during the LGC?
- 9 - Is the timing of glacial oscillations similar to that of the other Pyrenean, Iberian and European
10 mountain ranges?

11 12 **2. Study area**

13 The Pyrenees stretch from the Mediterranean Sea to the Bay of Biscay across ~450 km long and ~100 km
14 width and divide the Iberian and European tectonic plates. The geographical centre of the range coincides with
15 the highest peaks and a major hydrographic divide, where several rivers drain towards the northern (Aquitaine
16 Basin) and the southern (Ebro Basin) slopes.

17 The Upper Garonne constitutes one of the largest glacial catchments of the northern Central Pyrenees (1260
18 km²; Fernandes et al. 2017). It exceeds an elevation of 3,000 m in several peaks (e.g. Perdiguero Peak,
19 42°41'31''N-0°31'08'', 3,219 m; Maupas Peak, 3,111 m; Molières Peak, 3,009 m; Besiberri Nord Peak, 3,007
20 m) and reach 420-440 m at the frontal position of the PGC and LGC palaeoglaciers. The Ruda Valley, located
21 in the Aran Valley (Fig. 1B), constitutes the headwaters of the Garonne River that receives several other
22 tributaries downvalley to become one of the largest rivers of the Pyrenees; at the Tonneins River gauging
23 station, for example, the Garonne River reports an annual average discharge of 603 m³ s⁻¹ (1913-2013 series).
24 The abundant discharge results from the Atlantic climate regime, with high precipitation and moderate to cool
25 temperatures. Mean annual air temperature and annual precipitation range from 3 °C and 1,122 mm at the
26 Bonaigua station (2,266 m; 2000-2020 series) to 12 °C and 852 mm at Clarac (401 m; 2000-2020 series). The
27 precipitation rising and temperature dropping at higher elevations is controlled by the topography of the north
28 face of the range. The elevation difference (~2,800 m) of the catchment determines a wide range of snow
29 regimes: whereas snow remains in the ground over 8-10 months in the highest areas, the LBBb records scarce
30 snow fall (ANR SCAMPEI: http://www.umr-cnrm.fr/scampe/presentation_scampe/index.php).

31 The current landscape of the Pyrenees results from both tectonic dynamics and Pleistocene climatic oscillations
32 that have reshaped the environment through glacial, periglacial, alluvial, fluvial and slope processes (Oliva et
33 al. 2019). The LBBb is located at the foreland of the Pyrenees and it is flanked in the northern side by the
34 alluvial megafans of the Lannemezan Formation, which were built by the Neste River during the Late Neogene
35 (~10 Ma; Calvet et al. 2021). The margins of the basin are surrounded by small hills composed of Jurassic-
36 lower Cretaceous limestones standing 200-300 m above the basin floor, such as Picon Garros Peak (631 m),
37 Castillon Peak (684 m), Mail de Mau Bourg Peak (746 m), and le Picon Peak (777 m) (Fig. 1B). The
38 headwaters of the Garonne Valley are located in the Maladeta batholith, of Carboniferous age (granites and
39 granodiorites), while in the lower areas there are Cambrian to Devonian sedimentary (conglomerates,
40 limestones, lutites, sandstones) and metamorphic rocks (marbles, slates, schists, quartzites, hornfels; ICGC
41 2017; Quesada and Oliveira. 2019). Up waters, the Garonne Valley narrows and the river flows through steep
42 river gorges until the Marignac basin (490 m), which is surrounded by peaks up to 1,600 m (e.g. Cap de Pouy
43 de Hourmigué Peak 1,609 m). Currently, deciduous forest extends over most of the LBBb, particularly across
44 the surrounding hills and moraine ridges distributed on the basin floor. In the forest-free areas across the bottom
45 of the basin, cultivated fields and dispersed villages occupy the terraces built up by the Garonne River.

46
47
48
49
50
51
52 **Figure 1**

53 54 55 **3. Methodology**

56 The reconstruction of past glacial oscillations in the Upper Garonne Valley integrates geomorphological
57 observations, geochronological data, and palaeoglacier reconstructions. Field work was conducted during the
58 summer seasons of 2019 and 2020 to better identify the main geomorphological features and directly sample
59 glacial landforms for CRE dating.

3.1. Geomorphological mapping

Based on visual interpretation of satellite imagery from Google Earth®, orthophotomaps (0.5 cm resolution), 10-m resolution digital elevation model (DEM) from the ‘Institut National de L’information Geographique et Forestière’, the recent overviews of past glaciations in the Pyrenees (Delmas et al. 2021a and b) and on the *Carte géologique* 1:50,000 1054 N, BRGM (<https://www.geoportail.gouv.fr/>), a geomorphological map was produced focused on the glacial landforms extending across the area from the LBBb to the Marignac basin. This map was *in situ* validated and complemented with further field observations.

3.2. Sampling strategy related to CRE datings

After the geomorphological survey, 12 samples were collected from the main units highlighted in the aforementioned map for CRE dating following the standard procedures outlined in Gosse and Phillips (2001). Well-anchored moraine boulders of quartzite, granite and aplite and glacially polished bedrock surfaces (quartzite), were sampled for CRE dating. Sampling was restricted to flat-topped features and gentle surfaces (Table 1). Geometric correction of the topographic shielding by the surrounding topography was calculated throughout the ArcGIS toolbox based on the digital elevation model of 5 m resolution, which was devised by Li (2018).

Table 1

3.3. Laboratory procedures and CRE age calculation

After field work, samples were crushed and sieved to the 125-500 µm fraction, and subsequently, >200 g of it were chemically processed at the ‘Laboratoire National des Nucléides Cosmogéniques’ (LN₂C) of the ‘Centre Européen de Recherche et d’Enseignement des Géosciences de l’Environnement’ (CEREGE; Aix-en-Provence, France). According to the quartz-rich lithology, samples were processed for the extraction of the *in situ*-produced cosmogenic nuclide ¹⁰Be.

First, the magnetic minerals of the samples were discarded through magnetic separation conducted in a “Frantz LB-1” magnetic separator. After that, chemical attacks with a concentrated mixture of hydrochloric (1/3 HCl) and hexafluorosilicic (2/3 H₂SiF₆) acids and successive partial dissolutions with concentrated hydrofluoric acid (HF). Purified quartz was spiked with 150 µL of an in-house manufactured (from a phenakite crystal) ⁹Be carrier solution (3025 ± 9 µg ⁹Be g⁻¹; Merchel et al. 2008), then totally dissolved through a HF leaching, and finally Be was isolated using ion exchange columns (Merchel and Herpers 1999).

Final BeO targets were mixed with niobium powder and loaded in copper cathodes. Their ¹⁰Be/⁹Be ratios were measured in the ‘Accelerator pour les Sciences de la Terre, Environnement et Risques’ (ASTER) national AMS facility at CEREGE, from which the ¹⁰Be concentrations were inferred (Table 2). AMS measurements were calibrated against the in-house standard STD-11 with an assigned ¹⁰Be/⁹Be ratio of (1.191 ± 0.013) × 10⁻¹¹ (Braucher et al. 2015).

Table 2

¹⁰Be exposure ages were calculated using the CREp online calculator (Martin et al. 2017; <http://crep.crgp.cnrs-nancy.fr/#/>) with the following settings: LSD (Lifton-Sato-Dunai) elevation/latitude scaling scheme (Lifton et al. 2014), ERA40 atmospheric model (Uppala et al. 2005) and geomagnetic database based on the LSD framework (Lifton et al. 2014). The ‘world mean’ production rate derived from the ICE-D online calibration dataset (Martin et al. 2017; available online at: <http://calibration.ice-d.org/>) was chosen, which yielded a sea level high-latitude (SLHL) ¹⁰Be production rate of 3.98 ± 0.22 atoms g⁻¹ yr⁻¹. Exposure ages and 1σ full and analytical uncertainties of the samples are shown in Table 2. The uncertainties discussed throughout the text include analytical and production rate error unless otherwise stated.

In order to evaluate the potential impact of the erosion on the exposure ages, the same corrections outlined in Oliva et al. (2021) was implemented, which resulted in older ages by ~1% and ~8% for the 0.2 and 1 mm ka⁻¹ scenarios (André 2002), respectively. But aiming to enable comparisons with other areas the non-corrected ages was retained along the text. Snow cover is at present close to zero in the LBBb and is thus considered negligible. The high external and internal errors of the samples ARAN-05 and ARAN-81, linked to low current values during the AMS measurement implies that such samples and their derived exposure ages must be rejected. The chi-squared test was applied using the iceTEA tool (<http://ice-tea.org/en/tools/remove-outliers/>; Jones et al. 2019) to detect potential outliers within the targeted geomorphic units; thus, the exposure age of the sample ARAN-02 was excluded due to the statistical inconsistency.

3.4. Palaeoglaciers and PalaeELAs reconstruction

A three-dimensional palaeoglacier reconstruction was carried out for the different glacial phases using the 'GLaRe' ArcGIS toolbox developed by [Pellitero et al. \(2016\)](#) and a 10-m resolution DEM, which implements a perfect-plasticity physical-based numerical model ([Van der Veen 1999](#); [Benn and Hulton 2010](#)) that reconstructs past ice thickness assuming an average shear stress of 100 kPa along a set of flowlines ([Paterson 1994](#); [Benn and Hulton 2010](#)). And finally, equilibrium-line altitudes (ELAs) were calculated by using the automatic toolbox developed by [Pellitero et al. \(2015\)](#) through the methods Accumulation Area Ratio ([Porter 1975](#); AARs: 0.6 ± 0.05) and the Area Altitude Balance Ratio (AABR; [Osmaston 2005](#)). For more details on glacier reconstruction and ELA calculation protocols, the reader is referred to [Oliva et al. \(2021\)](#) and the original publications from which the aforementioned toolboxes were derived.

4. Results

The distribution of the glacial landforms preserved in the LBBb evidence several glacial advances and retreats during the Pleistocene (Fig. 2). Their timing is constrained by the ^{10}Be exposure ages obtained from moraine boulders and polished surfaces ([Tables 2 and 3](#)).

[Figure 2](#)

[Table 3](#)

4.1. Glacial geomorphological setting

Glacial deposits located in the LBBb have been largely transformed by historical human practices (e.g. agriculture) and by a dense network of infrastructures that have affected the natural landscapes and the preservation of glacial landforms. In addition, the entire area - particularly the slopes - is extensively forested, which makes even more challenging the interpretation of glacial features as well as the identification of appropriate samples for CRE dating (Fig. 3 and 4).

[Figure 3](#)

[Figure 4](#)

Nonetheless, based on our field work observations and on previous geomorphological mapping (*Carte géologique* 1:50,000 1054 N, BRGM; [Delmas et al. 2021a](#)), two main glacial systems were identified (Fig. 3):

- The external moraine system (EM)

There are only well-preserved deposits in the terminal zone of the palaeoglacier, downstream the villages of Izaourt and Tibiran-Juanac. It consists of the highest moraines of the EM in the internal and eastern parts of the basin and 4 moraine ridges in the western side of the basin floor (Fig. 4). The highest moraines of the EM are distributed on the slopes and hilltops of the internal part of the basin (Fig. 2b). At elevations between 600 and 720 m (i.e. 160-280 m above the basin floor) there are exposed sections opened on this moraine showing subangular to subrounded meter-sized granite and quartzite boulders embedded in a poorly sorted matrix. At the same altitude but close to Izaourt, several erratic granite boulders rest on a limestone bedrock that may correspond to the same phase (Fig. 3).

Further north, at lower altitudes (600-670 m), the highest moraines of the EM on the hilltop surface of the Castillon Peak do not define well-preserved moraine ridges, but patches of till deposits are located towards the eastern edge of the basin. Here, there are also sparse boulders and glaciofluvial sediments embedded in a sandy matrix. At the western side of the basin floor, moraines form aligned discontinuous ridges at 460-490 m (i.e. up to 40-70 m height), with well-developed soils and sparse boulders across the surface. These features are extensively forested. Up to four moraine ridges were identified in this system (Fig. 3 and 4A):

EM-1 - located at the northernmost part of the basin floor and represents the most peripheral moraine ridge preserved in the study area;

EM-2 - stretching between the Tibiran and Juanac villages, this ridge displays an oblique feature with regards to the palaeo ice-flow;

EM-3 - located 500 m to the south from the outer ridge, and turns from SW-NE to S-N towards Juanac village;

EM-4 - located 300 m north from the St-Martin village.

In order to validate the connection between the highest moraines close to the Castillon Peak and the external ridges near Tibiran-Juanac villages, the area was extensively surveyed to identify potential boulders suitable for CRE dating. Hubschman (1984) attributed those frontal moraines to glacial advances prior to the Eemian Interglacial. To test this hypothesis, 7 samples were collected from scattered moraine boulders belonging to the following units: the highest moraines of the EM (ARAN-03, ARAN-04), EM-2 (ARAN-01, ARAN-02) and EM-4 (ARAN-44, ARAN-45, ARAN-46). The few boulders found on EM-1 and EM-3 moraine ridges were not adequate for CRE dating as they had seemingly been disturbed from their original position, and therefore no samples were collected.

- The internal moraine system (IM)

A series of moraine ridges are distributed across the internal part of the LBBb floor at 460-590 m and the valley sides of the glacial catchment, at 550-820 m (Fig. 3), forming discontinuous ridges in the margins of the palaeoglacier. This well-preserved moraine system is composed of two sets of arches that are distributed on the LBBb and connects with lateral moraine ridges. Those moraine ridges are indicative of the frontal termination of the Garonne palaeoglacier in the LBBb and of the lateral margins where glacial deposits (ablation moraines and fluviolacustrine obturations) delineate large glacial diffluences that the Garonne palaeoglacier spread across the structural hills framed by the Jurassic-lower Cretaceous limestones of the North Pyrenean zone. Sedimentological, palynological and radiocarbon data obtained in the Barbazan glaciolacustrine sequence allow two main units to be distinguished within the LGC moraine system of the Garonne palaeoglacier (Fig. 3). Thus, two units were considered in the internal moraine system (Fig. 3):

IM-1 - In the terminal zone of the LBBb, IM-1 corresponds to a 5 km-long moraine preserved between Burs and St-Martin. Metric-size and well-anchored granite boulders were found in the Eastern margin of the moraine, lying on the foot slopes of Barbazan. Near Burs, the ridge rapidly decreases in elevation (from 590 to 490 m) towards the central part of the basin, connecting with a ~30-m-high arcuate frontal ridge at La Serre. In this section, and especially on the slope between Burs and the Barbazan paleolake, several sedimentary sequences contain meter-sized subrounded to rounded boulders of granite and quartzite, embedded in a sand and silt matrix. From the La Serre arch, the ridge turns westwards and ends 500 m next to the EM-4 ridge. In this section, several scattered boulders were detected at the north margin of the river and in south part of the St-Martin village. Only two samples were collected from the IM-1 ridge near Burs and Barbazan villages (ARAN-05, ARAN-07), at similar altitudes of 580 and 590 m (Table 1). On the lateral left moraine system, ~2 km upvalley from the LBBb, there are lateral ridges close to Aveux and Sacoué villages that are indicative of the palaeoglacier margins at the glacial diffluence. Further south, 6 km upvalley from the LBBb, frontal and lateral moraines lying between 620 and 800 m at the Sost-Ferrere glacial villages are also part of this moraine system. Finally, at the right moraine complex of the palaeoglacier margin, there are several lateral and frontal ridges distributed between 610 and 780 m near Lourde-St Pé d'Arde-Génos villages;

IM-2 - In the innermost part of the terminal zone of the LBBb, the IM-2 consists on two parallel moraine ridges (10 m high) located close to the current basin floor between Valcabrière, Labroquère and Loures-Barousse villages. Further south, in the moraine system of Sost-Ferrere, the most internal ridges standing at 580-600 m might correspond to the palaeoglacier margins of the IM-2. In the opposite side, this phase can be represented by lateral and frontal ridges at 530-610 m at the Lourde-St Pé d'Arde-Génos. Despite these lobate ridges surrounding the basin define well-preserved features, they have been intensely disturbed by agriculture activities. Therefore, no suitable boulders for CRE dating were found in the area as they were probably not in the original place where the ice left them.

Up-valley from the LBBb, the main valley narrows and no glacial features prone for CRE dating were found until the Marignac basin, 13 km upvalley, where the Garonne and la Pique rivers converge (Fig. 2). Hubschman (1984) attributed the IM-1 and IM-2 to glacial advances occurred during the LGC. At the left margin of the main Garonne Valley, there are polished surfaces on granite bedrock, at 18 km from the EM-1 ridge. In order

1 to validate Hubschman's interpretation, two samples were collected from these surfaces 50 and 30 m above
2 the riverbed (ARAN-42, ARAN-43), as representative of the age of the withdrawal of the palaeoglacier from
3 the terminal basin, of the lateral moraine complexes and of the individualization of the Garonne and la Pique
4 palaeoglaciers within their respective valleys.

4.2. CRE results

5 The 10 CRE samples collected from the LBBb yielded ages spanning from 128.5 ± 9.1 to 13.9 ± 1.5 ka (Table
6 2).

7
8 From the four moraine ridges integrating the EM moraine system, two samples were obtained from EM-2
9 (ARAN-01, ARAN-02) with inconsistent ages of 123.8 ± 8.0 and 41.7 ± 3.4 ka, respectively (Table 2). At the
10 EM-4 ridge, three samples (ARAN-44, ARAN-45, ARAN-46) yielded consistent ages of 127.9 ± 8.0 , $116.4 \pm$
11 9.4 and 128.5 ± 9.1 ka (mean age 124.3 ± 10.3 ka; $n=3$) (Fig. 3 and 5).
12

13 At the southern part of the LBBb, an erratic boulder located 240 m above the basin floor (ARAN-81) yielded
14 an age of 13.9 ± 1.5 ka. Due to the bad AMS measurement this age will not be further discussed. The highest
15 moraine of the EM loses altitude northwards, and at 230 and 220 m above the basin floor two other samples
16 were collected (ARAN-03 and ARAN-04) within a forest area near the Castillon Peak, yielding again
17 inconsistent exposure ages of 73.1 ± 4.6 and 31.1 ± 2.9 ka, respectively. (Fig. 3)
18

19 One sample collected from the IM-1 ridge, close to the Burs village (ARAN-05), reported an exposure age of
20 20.3 ± 12.7 ka. This age will not be further discussed. At the foot of the slopes surrounding the basin, another
21 sample (ARAN-07) was obtained near the Barbazan village and yielded an age of 17.1 ± 1.8 ka.
22

23 The exposure ages of two samples (ARAN-42, ARAN-43) obtained from polished surfaces in the
24 overdeepened basin surrounding the Marignac village, are 20.7 ± 1.2 and 24.2 ± 2.1 ka, respectively.
25

Figure 5

5. Discussion

26
27
28
29
30
31 The reconstruction of the glacial evolution in the LBBb is based on geomorphological surveying and mapping,
32 and ^{10}Be exposure ages obtained from moraine boulders and polished surfaces. Data confirms Hubschman's
33 proposal that the most weathered moraine (EM) was formed during a glacial advance prior the Eemian
34 Interglacial, as well as the onset of the final retreat of the Garonne Glacier during the gLGM.
35

5.1. Interpretation of the CRE results

36
37
38 The sequence of CRE ages from the terminal moraine system of the Upper Garonne Valley is constrained by
39 the long time since the penultimate deglaciation of the area and subsequent postglacial environmental
40 dynamics, which together with land use changes caused by humans within the last millennia in the LBBb, have
41 affected the preservation of the glacial records. Therefore, the reconstruction of the glacial history in the area
42 is challenging, and our study needs to be complemented with other environmental proxies and glacial
43 chronological data from the region.
44

45 The exposure ages of the samples (ARAN-01, ARAN-44, ARAN-45 and ARAN-46) from boulders distributed
46 on the moraine ridges EM-2 and EM-4 (123.8 ± 8.0 ka and 124.3 ± 10.3 ka, respectively) show statistical
47 consistence based on the Chi-2 test. They support the hypothesis that the oldest moraine system existing in the
48 glacial terminal basin of the Upper Garonne Valley corresponds to the PGC. These dates confirm the deposit
49 of those moraines during a glacial advance before the Eemian Interglacial period, as postulated in previous
50 studies (Hubschman 1984; Andrieu et al. 1988).
51

52 The exposure ages from the samples taken from the highest moraines of the EM (ARAN-03 and ARAN-04)
53 yielded 73.1 ± 4.6 and 31.1 ± 2.9 ka, respectively, showing a lack of consistency between them. These two
54 ages suggest that these moraines might correspond to polygenic features that formed over a long time period
55 when the glacier occupied the top of the Castillon Peak and finally shrunk by 31.1 ± 2.9 ka before the onset of
56 the Barbazan Lake infill, located 1.5 km south (Fig. 4-B; Andrieu et al. 1988). However, it is also likely that
57 our boulders had shifted from their original position by subsequent glacial advances or had been exhumated
58 by postglacial erosion processes occurring on the slopes of the Castillon Peak. Therefore, more data is needed
59
60
61
62
63
64
65

to confirm one of the scenarios and verify the link with the maximum glacial advance. Thus, given this uncertainty, for the reconstruction of the glacial history in the area, these samples were excluded.

The exposure age of 17.1 ± 1.8 ka (ARAN-07) obtained from the IM-1 moraine ridge near Burs must be excluded due to its mismatch with the Barbazan Lake records located upvalley, which indicates an older retreat than our exposure ages (Andrieu et al. 1988):

- (i) A radiocarbon age of 31.160 ± 1.700 yr BP (40.7-32.3 cal ka BP) at 2,263–2,274 cm (base of the core) within the basal unit (glaciolacustrine rhythmites and diamictons). Given the location of the Barbazan paleolake with respect to the IM-1, the area of the lake was covered by the ice when IM-1 was formed. Hence, this proglacial lake may only have infilled after the Garonne Glacier retreated from the IM-1. Hence, IM-1 should be older than 40.7-32.3 cal ka BP.
- (ii) The sedimentary frame of the glaciolacustrine sequence shows that the Garonne ice margin was close to the paleolake (probably at IM-2) until the interruption of glacial meltwater supply. This interruption occurred at 26.600 ± 460 yr BP (31.6-30.1 cal ka BP; Andrieu 1991), or just after 23.980 ± 680 yr BP (29.9-27.2 cal ka BP). It is however possible that the moraine boulders from the IM-1 ridge have been affected by reworking following ILGM glacial retreat and provide thus younger ages than expected.

New CRE ages from polished surfaces on the left margin of the Marignac basin (ARAN-42: 20.7 ± 1.2 ka and ARAN-43: 24.2 ± 2.1 ka) allow us to locate the terminal position of the Garonne palaeoglacier upstream of Marignac at the time of the gLGM.

5.2. Chronology of the glacial advances in the Upper Garonne Valley

Several smooth moraine ridges were mapped within the external moraine system of the LBBb, and ascribed to the oldest glacial advance in the area (Hubschman 1984; Andrieu 1991; Stange et al. 2014; Fernandes et al. 2017). Our CRE dates reveal two moraine ridges deposited prior to the LGC in the Upper Garonne Valley at 123.8 ± 8.0 and 124 ± 9.6 ka. Thus, four CRE dates from the EM-2 and EM-4 ridges provided evidence of moraine stabilization during a time interval spanning from 128.5 ± 9.1 to 116.4 ± 9.4 ka (Table 2). Isotopic inheritance is likely to be absent for moraines far from the source (~20-80 km), however the youngest ages might have been exhumated following the onset of moraine stabilization (Briner et al. 2005). Therefore, the oldest age of these units most likely marks the time of moraine stabilization following the MIS 6 largest glacial advance at ~129 ka. As temperatures increased during the transition toward the Eemian Interglacial (Helmens 2013), the Garonne Glacier started receding and moraines stabilized. This PGC glacial advance must have covered the entire glacial terminal basin of the Upper Garonne Valley with an ice thickness ranging between 200 to 50 m (Figure 6). According to our results, during this phase, the main Upper Garonne Glacier was ~78 km long and covered ~900 km². Considering the position of the frontal moraine ridge EM-2 at 480 m, and the derived palaeoglacier reconstruction, the ELA was located at $1,711 \pm -65/55$ m (AAR), $1,719 \pm -95/60$ m (global AABR) and $1,704 \pm -105/70$ m (mid-latitude AABR), with an average of 1,711 m. This altitude suggests a reduction of 9.3 °C with respect of current ELA at 3,139 m and assuming no change in the summer precipitation (Campos et al. 2021). As expected, these results show that glaciers had similar extents in the terminal basin during the MIS 6 and ILGM glacial advances and thus climate conditions were probably similar (Fernandes et al. 2017).

No solid chronological data are available to support a straightforward interpretation of the glacial advance during the PGC. The lack of available boulders for CRE dating in the EM-1 ridge impeded establishing the timing of the maximum extent during the PGC in the Upper Garonne Valley, whose external position on the moraine suggest that it may also belong to the PGC (Fig. 6). Indeed, there is evidence indicating that the Pyrenees were extensively glaciated during this period. In the Eastern Pyrenees, a stalagmitic flowstone stemmed from the onset of karst activity by 124.6 ± 6.9 to 121.4 ± 9.4 ka at the Niaux-Lombrives-Sabart cave occurred after the MIS 6 cold period (Sorriaux et al. 2016). In the same catchment, other age obtained from an erratic boulder located 50-100 m above the LGC moraines, reinforced the hypothesis of a previous glaciation that took place in the Ariège Valley at 133.9 ± 5.3 ka (Delmas et al. 2011). In the southern slope of the Pyrenees, an older age from the PGC has also been reported in the Aragón Valley where the outermost moraine, 80 m above the present-day riverbed, was dated at 171.0 ± 22.0 ka (García-Ruiz et al. 2013).

Geomorphological evidence from the LGC in the LBBb must thus be located in the internal part of the basin and foot slopes close to the Barbazan village. Here, the La Serre and the Burs ridges (IM-1) were generated by a piedmont glacier covering the basin during the ILGM of the LGC. The only available ages correspond to the

1 Barbazan Lake sequence, where the onset of the proglacial lake infill, behind this moraine, started before 40.7-
2 32.3 cal ka BP (Hubschman 1984; Andrieu 1991). In several valleys of the southern slope of the Pyrenees,
3 glacial evidence suggests that the ILGM occurred during the MIS 4 and MIS 3, namely at 65-55 ka and 45-30
4 ka (Oliva et al. 2019). However, the chronology of the ILGM glacial advances in the southern slope is not as
5 robust as in the northern slope. In the Ariège Valley, a CRE age from an erratic boulder located on the hilltop
6 between Tarascon and Foix-Montgaillard basins yielded 79.9 ± 14.3 ka and a boulder from a lateral moraine
7 on the confluence between the Aston and Ariège valleys yielded an exposure age of 35.3 ± 8.6 ka (Delmas et
8 al. 2011). In addition, radiocarbon dating of the first organic remnants from the bottom of the ice-marginal
9 deposits behind such moraines has shown the onset of the post-ILGM deglaciation between 48 and 24 ka,
10 namely at the Estarrès Lake, Gave d'Ossau ($34.2-29.7$ cal ka BP; Andrieu 1987; Andrieu et al. 1988; Jalut et
11 al. 1988), at the Biscaye peatbog, Gave de Pau ($48.3-39.7$ cal ka BP; Mardones and Jalut 1983), and at the
12 Freychinède sequence, Ariège Valley ($27.3-24.0$ cal ka BP; Jalut et al. 1982; Reille and Andrieu 1995).
13 Therefore, the ILGM glacial advance of the LGC in the LBBb is necessarily older than the onset of the
14 sedimentation at the Barbazan Lake, as the glaciolacustrine rhythmites and diamictos at the base of the core
15 sequence accumulated after the glacial retreat that followed the previous glacial advance, which likely
16 coincided with the formation of the IM-1 moraine. Glacial advances during the MIS 3 are more evident in the
17 Eastern Pyrenees, where moraines from Têt Valley were dated at 40.86 ± 1.9 ka (Tomkins et al. 2018) or those
18 in the Malniu area that yielded $51.1 \pm 4.8-42.6 \pm 4.1$ ka (Pallàs et al. 2010).

19 After the ILGM recession, a moraine-dammed lake formed between the IM-1 ridge and the glacier front
20 blocked the meltwater discharges and filled the Barbazan proglacial lake (Andrieu 1991). The same author
21 indicated that the glaciolacustrine rhythmites and diamictos at the bottom of the sequence ($40.7-32.3$ cal ka
22 BP) was transported from a nearby source, probably synchronously with the formation of the moraine IM-2.
23 However, no chronological data are yet available to discriminate whether the moraine was formed during a
24 pulsation after the ILGM or as a result of the gLGM advance. It can only be hypothesized that the ages must
25 be older than $31.6-30.1$ cal ka BP because sediments and pollen records showed the progressive glacial
26 abandonment of the terminal basin, with a transition from glaciolacustrine to lacustrine sediments, a reduction
27 of freshwater inputs from the glacier, as well as the decline of the forest coverage (e.g. *Fagus* sp.) and the
28 recovery of herbaceous species (Andrieu et al. 1988; Jalut et al. 1992).

29 The slopes surrounding the Marignac basin were ice-free during the gLGM, as demonstrated by the exposure
30 ages obtained from polished surfaces at 50 and 30 m above the basin floor. At 24-21 ka, the glacier would have
31 abandoned the terminal basin and split into two individualized glacier tongues constrained within the Garonne
32 and la Pique valleys as the ice shrank. At this time, the palaeoglacier of the Upper Garonne Valley flowed
33 down 60 km along the main valley. In parallel, glacial recession was also underway during the gLGM in the
34 Ariège Valley, where polished surfaces were dated to 18.7 ± 3.8 ka at 20 m above the gLGM Bompas moraine
35 (490 m) (Delmas et al. 2011). In this case the gLGM was depicted with glacial advances leaving several well-
36 preserved moraines (Garrabet, Bernière, Bompas-Arignac): a boulder from the Bernière frontal moraine, ~7
37 km from the ILGM ice limits was dated at 18.8 ± 1.3 ka (Delmas et al. 2011). Subsequently, after the gLGM,
38 glaciers in the Upper Garonne Valley underwent a massive retreat upvalley, reaching the mouth of the highest
39 cirques by ~15-14 ka (Oliva et al. 2021; Fernandes et al. 2021).

40 Figure 6

41 5.3. Mid-Late Pleistocene glacial dynamics in the Central Pyrenees in the context of European mid- 42 latitude regions

43 In Eurasia, climatic models have shown that the glacial maximum of the PGC was the most extensive of the
44 last 400 ka (Colleoni et al. 2016). This glacial maximum occurred at 140 ka (MIS 6) based on Antarctic ice
45 core records (Winograd et al. 1992; Colleoni et al. 2016), which is also confirmed by the minimum sea-level
46 (likely -150 m) dated at 155-140 ka (Grant et al. 2014; Wekerle et al. 2016). The Greenland ice core recorded
47 the Eemian Interglacial from 129 to 114 ka with a warming peak occurring at 126 ka (Dahl-Jensen et al. 2013).
48 These records correspond to a sea-level stabilization at 130-119 ka, reaching up to 6-9 m above the current
49 level (Hearty et al. 2007). According to the Greenland ice cores, this interglacial was up to 8 ± 4 °C warmer
50 than the last millennium (Dahl-Jensen et al. 2013). The beginning of the Eemian caused a massive ice discharge
51 from Northern Hemisphere ice sheets, when glaciers flowed into the ocean leaving icebergs that drifted debris
52 (>150 µm) southwards as far as ~55°N at 128 ka (McManus et al. 1999; Fig. 7). In fact, disintegration of the
53 northern ice sheets occurred during the end of the PGC, which coincided with the Heinrich Stadial 11 (~136-
54 129; Menviel et al. 2019).

Figure 7

According to marine sediments from the Iberian margins, a rapid warming with an increase of annual sea surface temperatures of ~ 10 °C followed the MIS 6 (Martrat et al. 2007). The comparison between the deep-sea cores in the Portuguese margins and European pollen records showed that in southwestern Iberia the warmest and driest period of this interglacial occurred between 126 and 117 ka (Sánchez-Goñi et al. 2005). Such warm conditions after the MIS 6 suggests non-favourable conditions to glacial development in the Iberian Peninsula. Consequently, it is likely that mid-latitude mountain glaciers, such as those existing in the Pyrenees, underwent a massive retreat leaving their terminal basins and probably the lowest peaks.

No robust chronological data on glacial records have been obtained so far to confirm the MIS 6 glaciation in the Pyrenees. Indeed, the wide temporal range (170-120 ka) of exposure ages and associated uncertainties do not let us to have a clear idea about the maximum of the PGC in the Pyrenees. In any case, in this work, the first ^{10}Be CRE dataset from moraine boulders was introduced in Pyrenees that reveal the occurrence of a large glaciation during the MIS 6 in the Upper Garonne Valley. At that time, the ice covered the terminal basin and the glacial system was more extensive than during the ILGM advance. The onset of the penultimate deglaciation started at ~ 129 ka, when the Garonne Glacier abandoned the two moraine ridges (EM-2 and EM-4) located at 480 m and they stabilized.

Intense postglacial geomorphic dynamics (glacial, periglacial, slope and alluvial) have eroded glacial landforms left by previous glaciations and therefore, the glacial evidence from MIS 6 in the Pyrenees can be only found in a few valleys. The glacial deposits beyond the limits of the LGC in this mountain range have been only recently ascribed to the PGC and gradually confirmed by optically stimulated luminescence (OSL) and CRE dating techniques (Oliva et al. 2019). These deposits, which are highly degraded, presenting only few scattered boulders suitable to CRE dating, are normally located in flat areas far from slope, periglacial and alluvial processes. Several studies have been published showing the glacial and karst evidence from the PGC in the Pyrenees and interpreted from the MIS 6 (Delmas et al. 2011; García-Ruiz et al. 2013; Sorriaux et al. 2016). Within the uncertainties, these evidences are also supported by a fluvial aggradation episode at 178 and 151 ka based on the existence of fluvial and fluvio-glacial sediments in fluvial terraces of the Cinca and Gállego valleys, respectively (Lewis et al. 2009).

Available dates of glacial processes during the PGC elsewhere in the Iberian Peninsula are also scarce. Similarly to what has happened with the LGC (Oliva et al. 2019), the increasing application of CRE methods is showing that the most extensive glaciers developed at the end of the PGC. CRE ages between 140 and 120 ka have been reported in several mountain regions regarding the most external moraines. This is the case of Sierra Nevada, where the lowest moraine was dated at 130-135 ka; Serra da Estrela, where the highest right lateral moraine was developed by ~ 140 ka; and even in the NW ranges, where a push moraine and a polished surface were dated at 155 and 131 ka (Table 4).

Table 4

Glacial evidence of the PGC has also been detected in other European mountains confirming the maximum glacial advance of the PGC during the MIS 6. This pattern occurred in the Alps, where one erratic boulder in the Jura Mountains was dated using two cosmogenic nuclides, ^{21}Ne and ^{10}Be , yielding 128 and 106 ka, respectively (Ivy-Ochs et al. 2006). In the Austrian Alps, OSL was applied to glaciofluvial, fluvio-lacustrine and eolian sediments showing a culmination of the PGC during the late MIS 6 (149-135 ka) (Bickel et al. 2015). Further south, very similar ages were obtained from U-series in the coastal mountains of the Adriatic Sea revealing cold conditions during the MIS 6, with moraine development starting at 125 ka in the Bijela Gora plateau (Hughes et al. 2010) and at 131 ka for the moraines from the Mount Tymphi, at the northern slope of the Pindus Mountains (Hughes et al. 2006).

During the gLGM, the terminal LBBb was ice free with the glaciers retreating towards headwaters at 24-21 ka. This is supported by exposure ages from polished surfaces, at 18 km southwards the EM-1 ridge, on the lower slopes of the Marignac overdeepened basin that became ice-free by that time (Fig. 7). Therefore, our results also introduce new chronological data about glacial dynamics occurring during the gLGM in the Central Pyrenees. In other valleys of this range, glaciers showed contrasting patterns of glacial advance or retreat during the gLGM. In the Eastern Pyrenees, a glacial advance occurred synchronous with the gLGM, that was noticed in the Têt Valley where a moraine at $\sim 1,690$ m was dated to 25 ka (Tomkins et al. 2018); and in the La Llosa and Duran valleys, where moraines at 1,520 m and at 1,830 m were dated to 20 and 21 ka, respectively

(Andrés et al. 2018). In the southern slope of the Pyrenees, glacial retreat was deduced in the upper sector of the Gállego Valley based on a paleolake located at ~1,500 m dammed by landslide by 20 ka (García-Ruiz et al. 2003).

In the Iberian Peninsula, a general glacial advance occurred at 22-19 ka followed by a massive recession (Oliva et al. 2019). In the central and northern part of the Iberia, other valleys also recorded glacial advances, such as in the Iberian Range, where the end of the gLGM was recorded based on lacustrine sediments in the Sierra de Neila was recorded prior to 21 ka (Vegas Salamanca 2007) or in NW ranges where the glacier front in the Tera Valley also remained stable until 22 cal ka BP (Rodríguez-Rodríguez et al. 2011). In the southern Iberian Peninsula, glaciers advanced during the gLGM in the Serra Nevada, where moraine stabilization in the San Juan Valley occurred at 21-19 ka (Palacios et al. 2016). In other European mountains, such as the Alps (Ivy-Ochs et al. 2008) or the at the Tatra Mountains (Engel et al. 2015), glaciers reached their maximum position of the LGC at 26-21 ka and undergone a subsequent massive retreat afterwards, at 20-19 ka. This suggests that the Garonne Glacier was already retreating when CO₂ concentrations in the atmosphere were still low (180-200 ppm; Shakun et al. 2015).

6. Conclusions

The Pyrenees hosted large ice fields during Quaternary glacial phases, with extensive alpine glaciers descending from the highest peaks of the axis of this mountain range. Those glaciers shaped the landscape and left a wide range of geomorphological features of glacial origin, both within the mountain range as well as in the surrounding lowlands of the northern slope. This is the case of the northern foreland of the Central Pyrenees at the LBBb. Here, the longest Late Pleistocene glacier in the Pyrenees that flowed northwards along ~80 km formed a terminal moraine system at only 420 m on its terminal position.

We present a 10-sample dataset of ¹⁰Be CRE dating providing ages for the Late Quaternary maximum ice extent as well as the extent of the Garonne glacier at the time of the gLGM. The long time passed since last deglaciation has favoured postglacial erosive processes and only a few stable boulders suitable for the application of CRE dating were found. Four boulders from the external moraine ridges confirm that the largest palaeoglacier in the Upper Garonne Valley developed before the LGC, at ~129 ka. These are the first CRE ages reporting a period of glacial expansion in the Pyrenees during the PGC, as also observed in other Iberian mountain ranges (e.g. Sierra Nevada, Central Range, NW Ranges) where the largest glacial advance during the MIS 6 was followed by a period of moraine stabilization at ~129 ka. However, boulders from the internal moraine system of the glacial terminal basin did not yield consistent geochronological results. Therefore, no data of glacial advance or retreat during the LGC is available in LBBb. Exposure ages from glacially polished bedrock surfaces located at the confluence Garonne-la Pique valleys - 18 km to the south of the external moraines - reported ages of 24-21 ka, confirming that the terminal basin was already ice-free during the gLGM.

A better understanding of glacial oscillations during glacial cycles prior to the last one is of major importance to assess whether the spatial and temporal trends of the last glaciation followed the same pattern observed in previous glaciations or they constitute a singular case during the Quaternary. Future research must provide further evidence of the occurrence of this glacial phase in the Pyrenees and couple it with environmental dynamics in the lowlands. The application of individual dating techniques does not resolve the full chronological sequence of the glacial oscillations during the PGC. Future research should address the combination of several data sources (fluvial, glacial, eolian, lacustrine, karst and archeological) and complement them with different chronological methods such as OSL and CRE dating to avoid the intrinsic limitations of each technique and circumvent the uncertainties associated with the occurrence of postglacial processes in such a dynamic environment.

Headings

- 1 **1. Introduction**
- 2 **2. Study area**
- 3 **3. Methodology**
 - 4 **3.1. Geomorphological mapping**
 - 5 **3.2. Sampling strategy related to CRE datings**
 - 6 **3.3. Laboratory procedures and CRE age calculation**
 - 7 **3.4. Palaeoglaciérs and PalaeoELAs reconstruction**
- 8 **4. Results**
 - 9 **4.1. Glacial geomorphological setting**
 - 10 **4.2. CRE results**
- 11 **5. Discussion**
 - 12 **5.1. Interpretation of the CRE results**
 - 13 **5.2. Chronology of the glacial advances in the Upper Garonne Valley**
 - 14 **5.3. Mid-Late Pleistocene glacial dynamics in the Central Pyrenees in the context of European**
 - 15 **mid-latitude regions**
- 16 **6. Conclusions**

Acknowledgements

21 The authors sincerely thank the Dr. Ramón Pellitero for his help to the construction of the Garonne
22 palaeoglaciérs. We also thank to anonymous reviewers for the constructive revision of an earlier draft of the
23 manuscript. The authors are grateful to Dr. Augusto Pérez-Alberti for his guidance and wise advices during
24 his prolific scientific career.

References

- 25
26
27
28
29
30 Adamson K, Hughes P, Woodward J (2013) Pleistocene glaciation of the Mediterranean Mountains. *Quat.*
31 *Newslett.* 131, 2–15.
- 32
33 Andrés N, Gómez-Ortiz A, Fernández-Fernández J.M, Tanarro García LM, Salvador- Franch F, Oliva M,
34 Palacios D (2018) Timing of deglaciation and rock glacier origin in the southeastern Pyrenees: a review
35 and new data. *Boreas* 47, 1050–1071. <https://doi.org/10.1111/bor.12324>
- 36
37 Andrieu V (1987) Le paléoenvironnement du piémont nord-pyrénéen occidental de 27 000 BP au
38 Postglaciaire: la séquence d'Estarrès (Pyrénées Atlantiques, France) dans le bassin glaciaire d'Arudy.
39 *Comptes-Rendus l'Académie des Sci.* 304, 103–108
- 40
41 Andrieu V (1991) Dynamique du paléoenvironnement de la vallée montagnarde de la Garonne (Pyrénées
42 centrales, France) de la fin des temps glaciaires à l'actuel. *Dissertation.* Toulouse 2.
- 43
44 Andrieu V, Hubschman J, Jalut G, Hérail G (1988) Chronologie de la déglaciation des Pyrénées françaises.
45 Dynamique de sédimentation et contenu pollinique des paléolacs ; application à l'interprétation du
46 retrait glaciaire. *Bull. l'Association française pour l'étude du Quat.* 25, 55–67
- 47
48 Bakalowicz M, Sorriaux P, Ford D (1984) Quaternary glacial events in the Pyrenees from U-series dating of
49 speleothems in the Niaux-Lombrives-Sabart caves, Ariège, France. *Nor. Geogr. Tidsskr.* 38, 193–197.
50 <https://doi.org/10.1080/00291958408552125>
- 51
52 Benn DI, Evans DJA (2010) *Glaciers and Glaciation*, second. ed, Hodder Education. London.
53 <https://doi.org/10.5860/CHOICE.35-6240>
- 54
55 Benn, DI, Hulton NRJ (2010) An Excel™ spreadsheet program for reconstructing the surface profile of
56 former mountain glaciers and ice caps. *Comput. Geosci.* 36, 605–610.
57 <https://doi.org/10.1016/j.cageo.2009.09.016>
- 58
59 Bernal-Wormull JL, Moreno A, Bartolomé M, Aranburu A, Arriolabengoa M, Iriarte E, Cacho I, Spötl C,
60 Edwards RL, Cheng H (2021) Immediate temperature response in northern Iberia to last deglacial
61 changes in the North Atlantic. *Geology* XX, 6–10. <https://doi.org/10.1130/G48660.1>

- 1 Bickel L, Lüthgens C, Lomax J, Fiebig M (2015) The timing of the penultimate glaciation in the northern
2 Alpine Foreland: New insights from luminescence dating. *Proc. Geol. Assoc.* 126, 536–550.
3 <https://doi.org/10.1016/j.pgeola.2015.08.002>
- 4 Briner, J, Kaufman, D, Manley, W, Finkel, R, Caffee, M (2005) Cosmogenic exposure dating of late
5 Pleistocene moraine stabilization in Alaska. *Geol. Soc. Am. Bull.* 117, 1108–1120.
6 <https://doi.org/10.1130/B25649.1>
- 7 Braucher R, Guillou V, Bourlès DL, Arnold M, Aumaître G, Keddadouche K, Nottoli E (2015) Preparation
8 of ASTER in-house $^{10}\text{Be}/^{9}\text{Be}$ standard solutions. *Nucl. Instruments Methods Phys. Res. Sect. B Beam*
9 *Interact. with Mater. Atoms* 361, 335–340. <https://doi.org/https://doi.org/10.1016/j.nimb.2015.06.012>
- 10 Calvet M (1996) Morphogenèse d'une montagne méditerranéenne: Les Pyrénées Orientales. Dissertation.
11 University of Orléans
- 12 Calvet M, Delmas M, Gunnell Y, Braucher R, Bourlès D (2011) Recent advances in research on quaternary
13 glaciations in the pyrenees. *Dev. Quat. Sci.* 15, 127–139. [https://doi.org/10.1016/B978-0-444-53447-](https://doi.org/10.1016/B978-0-444-53447-7.00011-8)
14 [7.00011-8](https://doi.org/10.1016/B978-0-444-53447-7.00011-8)
- 15 Calvet M, Gunnell Y, Laumonier B 2021. Denudation history and palaeogeography of the Pyrenees and their
16 peripheral basins: an 84-million-year geomorphological perspective. *Earth-Science Rev.* 215, 103436.
17 <https://doi.org/10.1016/j.earscirev.2020.103436>
- 18 Campos N, Alcalá-Reygosa J, Watson S, Kougkoulos I, Quesada-Román A, Grima N (2021) Modeling the
19 retreat of the Aneto Glacier (Spanish Pyrenees) since the Little Ice Age, and its accelerated shrinkage
20 over recent decades. *Holocene* 31, 1315–1326 <https://doi.org/10.1177/09596836211011678>
- 21 Colleoni F, Wekerle C, Näslund JO, Brandefelt J, Masina S (2016) Constraint on the penultimate glacial
22 maximum Northern Hemisphere ice topography (≈ 140 kyrs BP). *Quat. Sci. Rev.* 137, 97–112.
23 <https://doi.org/10.1016/j.quascirev.2016.01.024>
- 24 Copons R, Bordonau J (1996) El registro sedimentario del Cuaternario Reciente en el lago Redó
25 d'Aigüestortes (Pirineos Centrales), in: Grandal, A, Pagés, J. (Eds.), IV Reunión de Geomorfología.
26 Sociedad Española de Geomorfología
- 27 Crest Y, Delmas M, Braucher R, Gunnell Y, Calvet M (2017) Cirques have growth spurts during deglacial
28 and interglacial periods: Evidence from ^{10}Be and ^{26}Al nuclide inventories in the central and eastern
29 Pyrenees. *Geomorphology* 278, 60–77. <https://doi.org/10.1016/j.geomorph.2016.10.035>
- 30 Dahl-Jensen D, Albert MR, Aldahan A, Azuma N, Balslev-Clausen D, Baumgartner M, Berggren AM,
31 Bigler M, Binder T, Blunier T, Bourgeois JC, Brook EJ, Buchardt SL, Buizert C, Capron E, Chappellaz
32 J, Chung J, Clausen HB, Cvijanovic I, Davies SM, Ditlevsen P, Eicher O, Fischer H, Fisher DA, Fleet
33 LG, Gfeller G, Gkinis V, Gogineni S, Goto-Azuma K, Grinsted A, Gudlaugsdottir H, Guillevic M,
34 Hansen SB, Hansson M, Hirabayashi M, Hong S, Hur SD, Huybrechts P, Hvidberg CS, Iizuka Y, Jenk
35 T, Johnsen SJ, Jones TR, Jouzel J, Karlsson NB, Kawamura K, Keegan K, Kettner E, Kipfstuhl S, Kjær
36 HA, Koutnik M, Kuramoto T, Köhler P, Laepple T, Landais A, Langen PL, Larsen LB, Leuenberger D,
37 Leuenberger M, Leuschen C, Li J, Lipenkov V, Martinerie P, Maselli OJ, Masson-Delmotte V,
38 McConnell JR, Miller H, Mini O, Miyamoto A, Montagnat-Rentier M, Mulvaney R, Muscheler R, Orsi
39 AJ, Paden J, Panton C, Pattyn F, Petit JR, Pol K, Popp T, Possnert G, Prié F, Prokopiou M, Quiquet A,
40 Rasmussen SO, Raynaud D, Ren J, Reutenauer C, Ritz C, Röckmann T, Rosen JL, Rubino M, Rybak
41 O, Samyn, D, Sapart, C.J, Schilt, A, Schmidt, A.M.Z, Schwander, J, Schüpbach, S, Seierstad, I,
42 Severinghaus, J.P, Sheldon, S, Simonsen, S.B, Sjolte, J, Solgaard, A.M, Sowers, T, Sperlich, P, Steen-
43 Larsen, H.C, Steffen, K, Steffensen, J.P, Steinhage, D, Stocker, T.F, Stowasser, C, Sturevik AS,
44 Sturges WT, Sveinbjörnsdottir A, Svensson A, Tison JL, Uetake J, Vallelonga P, Van De Wal RSW,
45 Van Der Wel G, Vaughn BH, Vinther B, Waddington E, Wegner A, Weikusat I, White JWC, Wilhelms
46 F, Winstrup M, Witrant E, Wolff EW, Xiao C, Zheng J (2013) Eemian interglacial reconstructed from a
47 Greenland folded ice core. *Nature* 493, 489–494. <https://doi.org/10.1038/nature11789>
- 48 Delmas M, Gunnell Y, Braucher R, Calvet M, Bourlès D (2008) Exposure age chronology of the last
49 glaciation in the eastern Pyrenees. *Quat. Res.* 69, 231–241. <https://doi.org/10.1016/j.yqres.2007.11.004>
- 50 Delmas M, Calvet M, Gunnell Y, Braucher R, Bourlès D (2011) Palaeogeography and ^{10}Be exposure-age
51 chronology of Middle and Late Pleistocene glacier systems in the northern Pyrenees: Implications for
52
53
54
55
56

reconstructing regional palaeoclimates. *Palaeogeogr. Palaeoclimatol. Palaeoecol.* 305, 109–122.
<https://doi.org/10.1016/j.palaeo.2011.02.025>

- 1 Delmas M, Braucher R, Gunnell Y, Guillou V, Calvet M, Bourlès D (2015) Constraints on Pleistocene
2 glaciofluvial terrace age and related soil chronosequence features from vertical ^{10}Be profiles in the
3 Ariège River catchment (Pyrenees, France). *Glob. Planet. Change* 132, 39–53.
4 <https://doi.org/10.1016/j.gloplacha.2015.06.011>
5
- 6 Delmas M, Calvet M, Gunnell Y, Voinchet P, Manel C, Braucher R, Tissoux H, Bahain JJ, Perrenoud C,
7 Saos T (2018) Terrestrial ^{10}Be and electron spin resonance dating of fluvial terraces quantifies
8 quaternary tectonic uplift gradients in the eastern Pyrenees. *Quat. Sci. Rev.* 193, 188–211.
9 <https://doi.org/10.1016/j.quascirev.2018.06.001>
10
- 11 Delmas M, Gunnell Y, Calvet M, Reixach T, Oliva M (2021a) The Pyrenees: glacial landforms prior to the
12 Last Glacial Maximum. In: Palacios, D.; Hughes, P, García-Ruiz, J.M. & Andrés, N. (eds.). *European*
13 *Glacial Landscapes: Maximum Extent of Glaciations*. Elsevier
14
- 15 Delmas M, Gunnell Y, Calvet M, Reixach T, Oliva M (2021b) The Pyrenees: glacial landforms from the
16 Last Glacial Maximum. In: Palacios, D.; Hughes, P, García-Ruiz, J.M. & Andrés, N. (eds.). *European*
17 *Glacial Landscapes: Maximum Extent of Glaciations*. Elsevier
18
- 19 Ehlers J, Gibbard PL, Hughes PD (2011) Quaternary Glaciations - Extent and Chronology: A Closer Look.
20 *Developments in Quaternary Science*, 15. Elsevier, Amsterdam
21
- 22 Engel Z, Mentlik P, Baucher R, Minár J, Léanni L, Aster Team (2015) Geomorphological evidence and ^{10}Be
23 exposure ages for the Last Glacial Maximum and deglaciation of the Velká and Malá Studená dolina
24 valleys in the High Tatra Mountains, central Europe. *Quat. Sci. Rev.* 124, 106–123.
25 <http://dx.doi.org/10.1016/j.quascirev.2015.07.015>
26
- 27 Fernandes M, Oliva M, Palma P, Ruiz-Fernández J, Lopes L (2017) Glacial stages and post-glacial
28 environmental evolution in the Upper Garonne valley, Central Pyrenees. *Sci. Total Environ.* 584–585,
29 1282–1299. <https://doi.org/10.1016/j.scitotenv.2017.01.209>
30
- 31 Fernandes M, Oliva M, Vieira G, Palacios D, Fernández-Fernández JM, Garcia-Oteyza J, Schimmelpfennig
32 I, ASTER Team, Antoniades D (2021) Glacial oscillations during the Bølling-Allerød Interstadial-
33 Younger Dryas transition in the Ruda Valley, Central Pyrenees. *J. Quat. Sci.* doi: 10.1002/jqs.3379
34
- 35 Gangloff P, Hetu B, Courchesne F (1991) Présence d'un dépôt glaciaire sous la terrasse moyenne d'Agos,
36 vallée d'Aspe (Pyénées-Atlantiques). *Quaternaire* 2, 131–133. <https://doi.org/10.3406/quate.1991.1962>
37
- 38 García-Ruiz JM, Valero-Garcés BL, Martí-Bono C, González-Sampéris P (2003) Asynchronicity of
39 maximum glacier advances in the central Spanish Pyrenees. *J. Quat. Sci.* 18, 61–72.
40 <https://doi.org/10.1002/jqs.715>
- 41 García-Ruiz JM, Martí-Bono C, Peña-Monné J, Sancho C, Rhodes E, Valero-Garcés BL, González-Sampéris
42 P, Moreno A (2013) Glacial and Fluvial Deposits in the Aragón Valley, Central-Western Pyrenees:
43 Chronology of the Pyrenean Late Pleistocene Glaciers. *Geogr. Ann. Ser. A Phys. Geogr.* 95, 15–32.
44 <https://doi.org/10.1111/j.1468-0459.2012.00478.x>
45
- 46 González-Sampéris P, Valero-Garcés BL, Moreno A, Jalut G, García-Ruiz JM, Martí-Bono C, Delgado-
47 Huertas A, Navas A, Otto T, Dedoubat J (2006) Climate variability in the Spanish Pyrenees during the
48 last 30,000 yr revealed by the El Portalet sequence. *Quat. Res.* 66, 38–52.
49 <https://doi.org/10.1016/j.yqres.2006.02.004>
50
- 51 Gosse J, Philips F (2001) Terrestrial in situ cosmogenic nuclides: theory and application. *Quat. Sci. Rev.* 20,
52 1475–1560. [https://doi.org/10.1016/S0277-3791\(00\)00171-2](https://doi.org/10.1016/S0277-3791(00)00171-2)
53
- 54 Gourinard Y (1971) Les moraines de la basse vallée du Carol entre Latour et Puiccerda (Pyénées orientales
55 franco-espagnoles). *Compte Rendu Académie des Sci.* 272, 3112–3115
56
- 57 Grant KM, Rohling EJ, Bronk Ramsey C, Cheng H, Edwards RL, Florindo F, Heslop D, Marra F, Roberts
58 AP, Tamisiea ME, Williams F (2014) Sea-level variability over five glacial cycles. *Nat. Commun.* 5.
59 <https://doi.org/10.1038/ncomms6076>
60
- 61 Hearty PJ, Hollin JT, Neumann AC, O'Leary MJ, McCulloch M (2007) Global sea-level fluctuations during
62
63
64
65

the Last Interglaciation (MIS 5e). *Quat. Sci. Rev.* 26, 2090–2112.
<https://doi.org/10.1016/j.quascirev.2007.06.019>

- 1 Hétu B, Gangloff P (1989) Dépôts glaciaires du Pléistocène inférieur sur le piémont des Pyrénées
2 Atlantiques. *Zeitschrift für Geomorphol.* 33, 384–403
3
- 4 Hétu B, Gangloff P, Courchesne F (1992) Un till de déformation du Pléistocène inférieur à la base de la
5 Formation du Lannemezan (Piémont des Pyrénées Atlantiques, France). *Quaternaire* 3, 53–61
6
- 7 Hubschman J (1975) Conclusion : Evolution pédo-géochimique et interprétation paléobioclimatique de
8 piémont quaternaire garonnais. *Bull. l'Association française pour l'étude du Quat.* 12, 211–216
9
- 10 Hubschman J (1984) Glaciaire ancien et glaciaire récent: analyse comparée de l'altération de moraines
11 terminales nord-pyrénéennes. *Mont. Piémonts R.G.P.S.O.* 313–332
- 12 Hughes PD, Woodward JC, Gibbard PL, Macklin MG, Gilmour MA, Smith GR (2006) The glacial history of
13 the Pindus Mountains, Greece. *J. Geol.* 114, 413–434. <https://doi.org/10.1086/504177>
14
- 15 Hughes P, Woodward JC, van Calsteren PC, Thomas AL, Adamson KR (2010) Pleistocene ice caps on the
16 coastal mountains of the Adriatic Sea. *Quat. Sci. Rev.* 29, 3690–3708.
17 <https://doi.org/10.1016/j.quascirev.2010.06.032>
18
- 19 ICGC (2017) Base de données géologiques de Catalunya 1:50.000 v1.0.
- 20
- 21 Ivy-Ochs S, Kerschner H, Reuther A, Maisch M, Sailer R, Schaefer J, Kubik PW, Synal H, Schlüchter C
22 (2006) The timing of glacier advances in the northern European Alps based on surface exposure dating
23 with cosmogenic ^{10}Be , ^{26}Al , ^{36}Cl , and ^{21}Ne . *Geol. Soc. Am. Spec. Pap.* 415, 43–60.
24 [https://doi.org/10.1130/2006.2415\(04\)](https://doi.org/10.1130/2006.2415(04))
- 25
- 26 Ivy-Ochs S, Kerschner H, Reuther A, Preusser F, Heine K, Maisch M, Kubik P, Schlüchter C (2008)
27 Chronology of the last glacial cycle in the European Alps. *Journal of Quaternary Science* 22, 559–573.
28 <https://doi.org/10.1002/jqs.1202>
- 29
- 30 Jalut G, Delibrias G, Dagnac J, Mardones M, Bouhours M (1982) A palaeoecological approach to the last 21
31 000 years in the pyrenees: The peat bog of Freychinède (Alt. 1350 m, Ariège, South France).
32 *Palaeogeogr. Palaeoclimatol. Palaeoecol.* 40, 321–359. [https://doi.org/10.1016/0031-0182\(82\)90033-5](https://doi.org/10.1016/0031-0182(82)90033-5)
- 33
- 34 Jalut G, Andrieu V, Delibrias G, Fontugne M (1988) Palaeoenvironment of the valley of Ossau (Western
35 French Pyrenees) during the last 27,000 years. *Pollen et spores* 30, 357–394
- 36
- 37 Jalut G, Monserrat-Martí J, Fontugne M, Delibrias G, Vilaplana J, Rosen J (1992) Glacial to interglacial
38 vegetation changes in the northern and southern Pyrénées: deglaciation, vegetation cover and
39 chronology. *Quat. Sci. Rev.* 11, 449–480
- 40
- 41 Jones RS, Small D, Cahill N, Bentley MJ, Whitehouse PL (2019) iceTEA: Tools for plotting and analysing
42 cosmogenic-nuclide surface-exposure data from former ice margins. *Quat. Geochronol.* 51, 72–86.
43 <https://doi.org/10.1016/j.quageo.2019.01.001>
- 44
- 45 Lewis CJ, McDonald EV, Sancho C, Peña JL, Rhodes EJ (2009) Climatic implications of correlated Upper
46 Pleistocene glacial and fluvial deposits on the Cinca and Gállego Rivers (NE Spain) based on OSL
47 dating and soil stratigraphy. *Glob. Planet. Change* 67, 141–152.
48 <https://doi.org/10.1016/j.gloplacha.2009.01.001>
- 49
- 50 Li Y (2018) Determining topographic shielding from digital elevation models for cosmogenic nuclide
51 analysis: a GIS model for discrete sample sites. *J. Mt. Sci.* 15, 939–947.
52 <https://doi.org/10.1007/s11629-018-4895-4>
- 53
- 54 Lisiecki L, Raymo M (2005) A Pliocene-Pleistocene stack of 57 globally distributed benthic $\delta^{18}\text{O}$ records.
55 *Paleoceanography* 20, 1–7. <https://doi.org/10.1029/2004PA001071>
- 56
- 57 Lifton N, Sato T, Dunai T (2014) Scaling in situ cosmogenic nuclide production rates using analytical
58 approximations to atmospheric cosmic-ray fluxes. *Earth Planet. Sci. Lett.* 386, 149–160.
59 <https://doi.org/10.1016/j.epsl.2013.10.052>
- 60
- 61 Mardones M, Jalut G (1983) La tourbière de Biscaye (alt. 409 m, Hautes Pyrénées): Approche
62 paléocologique des 45.000 dernières années. *Pollen et spores* 25, 163–212
63
64
65

- 1 Martin LCP, Blard PH, Balco G, Lavé J, Delunel R, Lifton N, Laurent V (2017) The CREp program and the
2 ICE-D production rate calibration database: A fully parameterizable and updated online tool to compute
3 cosmic-ray exposure ages. *Quat. Geochronol.* 38, 25–49.
4 <https://doi.org/10.1016/J.QUAGEO.2016.11.006>
- 5 Martrat B, Grimalt JO, Shackleton NJ, De Abreu L, Hutterli MA, Stocker TF (2007) Four climate cycles of
6 recurring deep and surface water destabilizations on the Iberian margin. *Science* (80-) 317, 502–507.
7 <https://doi.org/10.1126/science.1139994>
- 8 McManus JF, Oppo DW, Cullen JL (1999) A 0.5-Million-year record of millennial-scale climate variability
9 in the North Atlantic. *Science* (80-) 283, 971–975. <https://doi.org/10.1126/science.283.5404.971>
- 10 Menviel L, Capron E, Govin A, Dutton A, Tarasov L, Abe-Ouchi A, Drysdale RN, Gibbard PL, Gregoire L,
11 He F, Ivanovic RF, Kageyama M, Kawamura K, Landais A, Otto-Bliesner BL, Oyabu I, Tzedakis PC,
12 Wolff E, Zhang X (2019) The penultimate deglaciation: Protocol for Paleoclimate Modelling
13 Intercomparison Project (PMIP) phase 4 transient numerical simulations between 140 and 127 ka,
14 version 1.0. *Geosci. Model Dev.* 12, 3649–3685. <https://doi.org/10.5194/gmd-12-3649-2019>
- 15 Merchel S, Herpers U (1999) An Update on Radiochemical Separation Techniques for the Determination of
16 Long-Lived Radionuclides via Accelerator Mass Spectrometry. *Radiochim. Acta* 84, 215–219.
17 <https://doi.org/10.1524/ract.1999.84.4.215>
- 18 Merchel S, Arnold M, Aumaître G, Benedetti L, Bourlès DL, Braucher R, Alfimov V, Freeman SPHT, Steier
19 P, Wallner A (2008) Towards more precise ¹⁰Be and ³⁶Cl data from measurements at the 10-14 level:
20 Influence of sample preparation. *Nucl. Instruments Methods Phys. Res. Sect. B Beam Interact. with*
21 *Mater. Atoms* 266, 4921–4926. <https://doi.org/10.1016/j.nimb.2008.07.031>
- 22 Montserrat J (1992) Evolución glacial y postglacial del clima y la vegetación en la vertiente sur del Pirineo:
23 estudio palinológico. *Monogr. del Inst. Piren. Ecol. Actas. Instituto Pirenaico de Ecología*
- 24 Morellón M, Valero-Garcés B, Vegas-Vilarrúbia T, González-Sampériz P, Romero Ó, Delgado-Huertas A,
25 Mata P, Moreno A, Rico M, Corella JP (2009) Lateglacial and Holocene palaeohydrology in the
26 western Mediterranean region: The Lake Estanya record (NE Spain). *Quat. Sci. Rev.* 28, 2582–2599.
27 <https://doi.org/10.1016/j.quascirev.2009.05.014>
- 28 Obrochta S, Crowley T, Channell J, Hodell D, Baker P, Seki A, Yokoyama Y (2014) Climate variability and
29 ice-sheet dynamics during the last three glaciations. *Earth Planet. Sci. Lett.* 406, 198–212.
30 <https://doi.org/10.1016/j.epsl.2014.09.004>
- 31 Oliva M, Palacios D, Fernández-Fernández JM, Rodríguez-Rodríguez L, García-Ruiz JM, Andrés N,
32 Carrasco RM, Pedraza J, Pérez-Alberti A, Valcárcel M, Hughes P (2019) Late Quaternary glacial
33 phases in the Iberian Peninsula. *Earth-Science Rev.* 192, 564–600.
34 <https://doi.org/10.1016/j.earscirev.2019.03.015>
- 35 Oliva M, Fernandes M, Palacios D, Fernández-Fernández JM, Schimmelpfennig I, Team ASTER,
36 Antoniadou D (2021) Rapid deglaciation during the Bølling-Allerød Interstadial in the Central Pyrenees
37 and associated glacial and periglacial landforms. *Geomorphology* 107735.
38 <https://doi.org/10.1016/j.geomorph.2021.107735>
- 39 Osmaston H (2005) Estimates of glacier equilibrium line altitudes by the Area×Altitude, the Area×Altitude
40 Balance Ratio and the Area×Altitude Balance Index methods and their validation. *Quat. Int.* 138–139,
41 22–31. <https://doi.org/10.1016/j.quaint.2005.02.004>
- 42 Palacios D, Andrés N, López-Moreno JI, García-Ruiz JM (2015a) Late Pleistocene deglaciation in the upper
43 Gállego Valley, central Pyrenees. *Quat. Res. (United States)* 83, 397–414.
44 <https://doi.org/10.1016/j.yqres.2015.01.010>
- 45 Palacios D, Gómez-Ortiz A, Andrés N, Vázquez-Selem L, Salvador- Franch F, Oliva M (2015b) Maximum
46 extent of Late Pleistocene glaciers and last deglaciation of La Cerdanya mountains, Southeastern
47 Pyrenees. *Geomorphology* 231, 116–129. <https://doi.org/10.1016/j.geomorph.2014.10.037>
- 48 Palacios D, Gómez-Ortiz A, Andrés N, Salvador- Franch F, Oliva M (2016) Timing and new
49 geomorphologic evidence of the last deglaciation stages in Sierra Nevada (southern Spain). *Quat. Sci.*
50 *Rev.* 150, 110–129. <https://doi.org/10.1016/j.quascirev.2016.08.012>

- 1
2
3
4
5
6
7
8
9
10
11
12
13
14
15
16
17
18
19
20
21
22
23
24
25
26
27
28
29
30
31
32
33
34
35
36
37
38
39
40
41
42
43
44
45
46
47
48
49
50
51
52
53
54
55
56
57
58
59
60
61
62
63
64
65
- Palacios D, García-Ruiz JM, Andrés N, Schimmelpfennig I, Campos N, Léanni L, Aumaître G, Bourlès DL, Keddadouche K (2017) Deglaciation in the central Pyrenees during the Pleistocene–Holocene transition: Timing and geomorphological significance. *Quat. Sci. Rev.* 162, 111–127. <https://doi.org/10.1016/j.quascirev.2017.03.007>
- Pallàs R, Rodés Á, Braucher R, Carcaillet J, Ortuño M, Bordonau J, Bourlès D, Vilaplana JM, Masana E, Santanach P (2006) Late Pleistocene and Holocene glaciation in the Pyrenees: a critical review and new evidence from ¹⁰Be exposure ages, south-central Pyrenees. *Quat. Sci. Rev.* 25, 2937–2963. <https://doi.org/10.1016/j.quascirev.2006.04.004>
- Pallàs R, Rodés Á, Braucher R, Bourlès D, Delmas M, Calvet M, Gunnell Y (2010) Small, isolated glacial catchments as priority targets for cosmogenic surface exposure dating of Pleistocene climate fluctuations, southeastern Pyrenees. *Geology* 38, 891–894. <https://doi.org/10.1130/G31164.1>
- Paterson WSB (1994) *The Physics of Glaciers*, 3rd Editio. ed. Elsevier, London. <https://doi.org/10.1016/C2009-0-14802-X>
- Pearce D, Ely J, Barr I, Boston C (2017) *Glacier Reconstruction*, in: Cook, S, Clarke, L, Nield, J. (Eds.), *Geomorphological Techniques*. British Society for Geomorphology
- Pellitero R, Rea BR, Spagnolo M, Bakke J, Hughes P, Ivy-Ochs S, Lukas S, Ribolini A (2015) A GIS tool for automatic calculation of glacier equilibrium-line altitudes. *Comput. Geosci.* 82, 55–62. <https://doi.org/10.1016/j.cageo.2015.05.005>
- Pellitero R, Rea BR, Spagnolo M, Bakke J, Ivy-Ochs S, Frew CR, Hughes P, Ribolini A, Lukas S, Renssen H (2016) GlaRe, a GIS tool to reconstruct the 3D surface of palaeoglaciers. *Comput. Geosci.* 94, 77–85. <https://doi.org/10.1016/j.cageo.2016.06.008>
- Porter SC (1975) Equilibrium-line altitudes of late Quaternary glaciers in the Southern Alps, New Zealand. *Quat. Res.* 5, 27–47. [https://doi.org/10.1016/0033-5894\(75\)90047-2](https://doi.org/10.1016/0033-5894(75)90047-2)
- Quesada C, Oliveira J (2019) *The Geology of Iberia: A Geodynamic Approach: The Variscan Cycle*.
- Quinif Y, Maire R (1998) Pleistocene deposits in Pierre Saint-Martin cave, French Pyrenees. *Quat. Res.* 49, 37–50. <https://doi.org/10.1006/qres.1997.1939>
- Rasmussen S.O, Bigler M, Blockley SP, Blunier T, Buchardt SL, Clausen HB, Cvijanovic I, Dahl-Jensen D, Johnsen SJ, Fischer H, Gkinis V, Guillevic M, Hoek WZ, Lowe JJ, Pedro JB, Popp T, Seierstad IK, Steffensen JP, Svensson AM, Vallenga P, Vinther BM, Walker MJC, Wheatley JJ, Winstrup M (2014) A stratigraphic framework for abrupt climatic changes during the Last Glacial period based on three synchronized Greenland ice-core records: Refining and extending the INTIMATE event stratigraphy. *Quat. Sci. Rev.* 106, 14–28. <https://doi.org/10.1016/j.quascirev.2014.09.007>
- Reille M, Andrieu V (1995) The late Pleistocene and Holocene in the Lourdes Basin, Western Pyrenees, France: new pollen analytical and chronology data. *Veg. Hist. Archaeobot.* 4, 1–21
- Reixach T, Delmas M, Calvet M (2021) Climatic conditions between 19 and 12 ka in the eastern Pyrenees, and wider implications for atmospheric circulation patterns in Europe. *Quat. Sci. Rev.* 260. <https://doi.org/10.1016/j.quascirev.2021.106923>
- Rodríguez-Rodríguez L, Jiménez-Sánchez M, Domínguez-Cuesta MJ, Rico MT, Valero-Garcés B (2011) Last deglaciation in northwestern Spain: New chronological and geomorphologic evidence from the Sanabria region. *Geomorphology* 135, 48–65. <https://doi.org/10.1016/j.geomorph.2011.07.025>
- Sánchez-Goñi MF, Loutre MF, Crucifix M, Peyron O, Santos L, Duprat J, Malaizé B, Turon JL, Peypouquet JP (2005) Increasing vegetation and climate gradient in Western Europe over the Last Glacial Inception (122–110 ka): Data-model comparison. *Earth Planet. Sci. Lett.* 231, 111–130. <https://doi.org/10.1016/j.epsl.2004.12.010>
- Sancho C, Arenas C, Pardo G, Peña-Monné JL, Rhodes EJ, Bartolomé M, García-Ruiz JM, Martí-Bono C (2018) Glaciolacustrine deposits formed in an ice-dammed tributary valley in the south-central Pyrenees: New evidence for late Pleistocene climate. *Sediment. Geol.* 366, 47–66. <https://doi.org/10.1016/j.sedgeo.2018.01.008>
- Shakun JD, Clark PU, He F, Lifton NA, Liu Z, Otto-Bliesner BL (2015) Regional and global forcing of

glacier retreat during the last deglaciation. *Nat. Commun.* 6, 1–7. <https://doi.org/10.1038/ncomms9059>

- 1
2
3
4
5
6
7
8
9
10
11
12
13
14
15
16
17
18
19
20
21
22
23
24
25
26
27
28
29
30
31
32
33
34
35
36
37
38
39
40
41
42
43
44
45
46
47
48
49
50
51
52
53
54
55
56
57
58
59
60
61
62
63
64
65
- Sorriaux P, Delmas M, Calvet M, Gunnell Y, Durand N, Edwige P (2016) Relations entre karst et glaciers depuis 450 ka dans les grottes de Niaux-Lombrives-Sabart (Pyrénées ariégeoises) Nouvelles datations U/Th dans la grotte de Niaux. *Karstologia* 67, 3–16
- Stange KM, van Balen RT, Kasse C, Vandenberghe J, Carcaillet J (2014) Linking morphology across the glaciofluvial interface: A ^{10}Be supported chronology of glacier advances and terrace formation in the Garonne River, northern Pyrenees, France. *Geomorphology* 207, 71–95. <https://doi.org/10.1016/j.geomorph.2013.10.028>
- Tomkins MD, Dortch JM, Hughes PD, Huck JJ, Stimson AG, Delmas M, Calvet M, Pallàs R (2018) Rapid age assessment of glacial landforms in the Pyrenees using Schmidt hammer exposure dating (SHED). *Quat. Res. (United States)* 90, 26–37. <https://doi.org/10.1017/qua.2018.12>
- Turu V, Peña-Monné JL (2006) Las terrazas fluviales del sistema Segre-Valira (Andorra-La Seu d’Urgell- Organyà, Pirineos Orientales): relación con el glaciario y la tectónica activa. *Geomorfol. y Territ.* 113–128
- Turu V, Boulton GS, Ros I, Visus X, Peña- Monné JL, Martí-Bono C, Ibern JBI, Serrano- Cañadas E, Sancho- Marcén C, Constante-Orrios A, Pous Fàbregas J, Gonzalez- Trueba JJ, Palomar Molins J, Herrero Simón R, García- Ruiz JM (2007) Structure des grands bassins glaciaires dans le nord de la péninsule ibérique : comparaison entre les vallées d’Andorre (Pyrénées orientales), du Gallego (Pyrénées centrales) et du Trueba (Chaîne cantabrique). *Quaternaire* 309–325. <https://doi.org/10.4000/quaternaire.1167>
- Turu V, Calvet M, Bordonau J, Gunnell Y, Delmas M, Vilaplana J, Jalut G (2016) Did Pyrenean glaciers dance to the beat of global climatic events? Evidence from the Würmian sequence stratigraphy of an ice-dammed palaeolake depocentre in Andorra. *Geol. Soc. London, Spec. Publ.* 433, 111–136. <https://doi.org/10.1144/sp433.6>
- Uppala SM, Kållberg PW, Simmons AJ, Andrae U, da Costa Bechtold V, Fiorino M, Gibson JK, Haseler J, Hernandez A, Kelly GA, Li X, Onogi K, Saarinen S, Sokka N, Allan RP, Andersson E, Arpe K, Balmaseda MA, Beljaars ACM, van de Berg L, Bidlot J, Bormann N, Caires S, Chevallier F, Dethof A, Dragosavac M, Fisher M, Fuentes M, Hagemann S, Hólm E, Hoskins BJ, Isaksen I, Janssen PAEM, Jenne R, McNally AP, Mahfouf JF, Morcrette JJ, Rayner NA, Saunders RW, Simon P, Sterl A, Trenberth KE, Untch A, Vasiljevic D, Viterbo P, Woollen J (2005) The ERA-40 re-analysis. *Q. J. R. Meteorol. Soc.* 131, 2961–3012. <https://doi.org/10.1256/qj.04.176>
- Van der Veen C (1999) *Fundamentals of Glaciers Dynamics*, Second Edi. ed. Balkema, Rotterdam.
- Vegas Salamanca J (2007) Caracterización de eventos climáticos del Pleistoceno superior-Holoceno mediante el estudio sedimentológico de la Laguna Grande (Sierra Neila, NO Sistema Ibérico). *Rev. la Soc. Geológica España* 20, 53–70.
- Wekerle C, Colleoni F, Näslund JO, Brandefelt J, Masina S (2016) Numerical reconstructions of the penultimate glacial maximum Northern Hemisphere ice sheets: Sensitivity to climate forcing and model parameters. *J. Glaciol.* 62, 607–622. <https://doi.org/10.1017/jog.2016.45>
- Winograd IJ, Coplen TB, Landwehr JM, Riggs AC, Ludwig KR, Szabo BJ, Kolesar PT, Revesz KM (1992) Continuous 500,000-year climate record from vein calcite in Devils Hole, Nevada. *Science (80-.)*. 258, 255–260. <https://doi.org/10.1126/science.258.5080.255>

List of figures

1 Figure 1. Location of the terminal basin of the Loures-Barousse-Barbazan (C) in the Pyrenees (B) and Europe
2 (A).

3 Figure 2. Examples of the samples collected from the polished surface in the Marignac basin (A; ARAN-42),
4 and the erratic boulder (B; ARAN-81) and moraine boulder (C; ARAN-45) from the Loures-Barousse-
5 Barbazan basin.

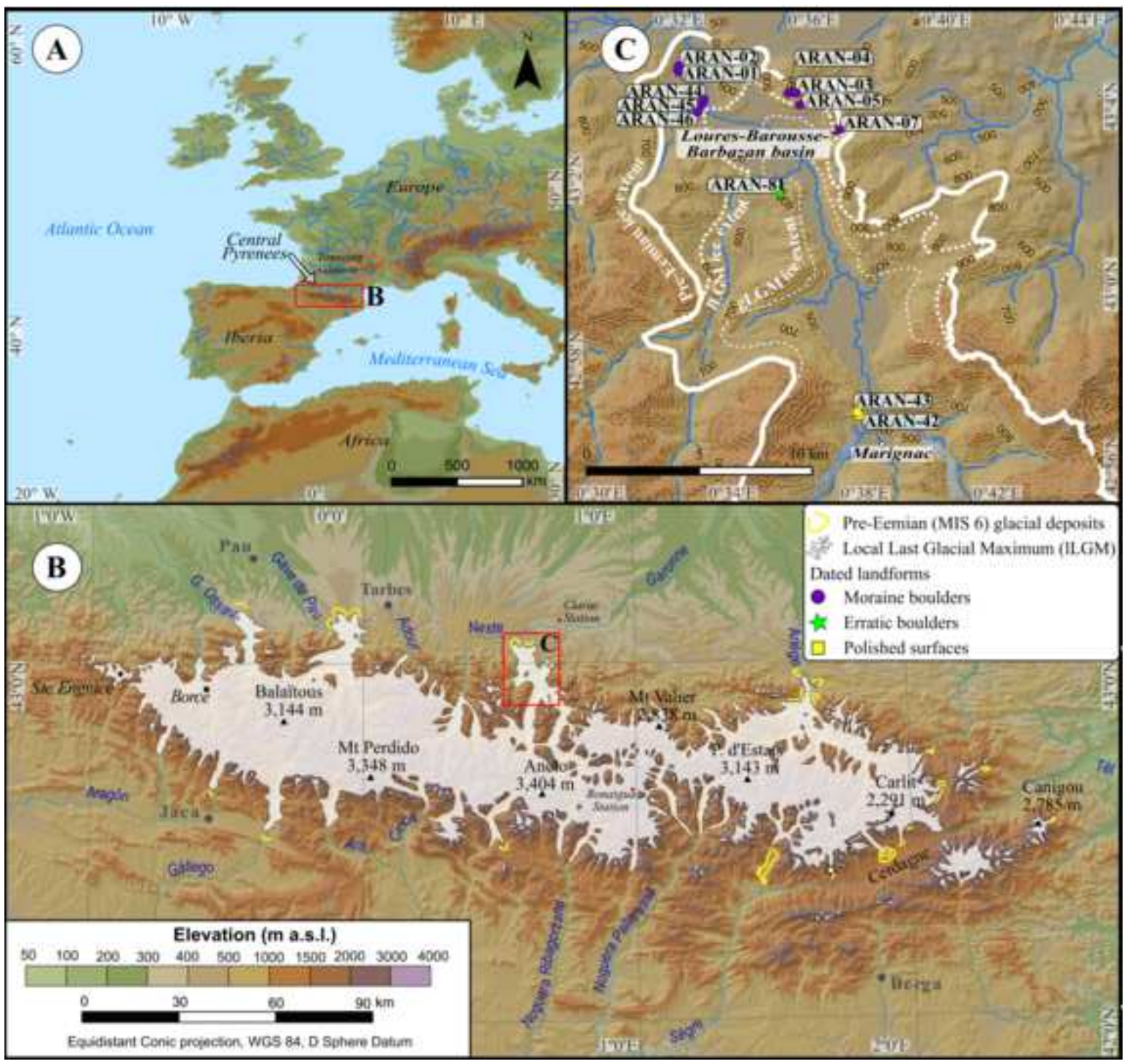
6 Figure 3. Geomorphological map of the study area modified from Delmas et al. (2021a, b).

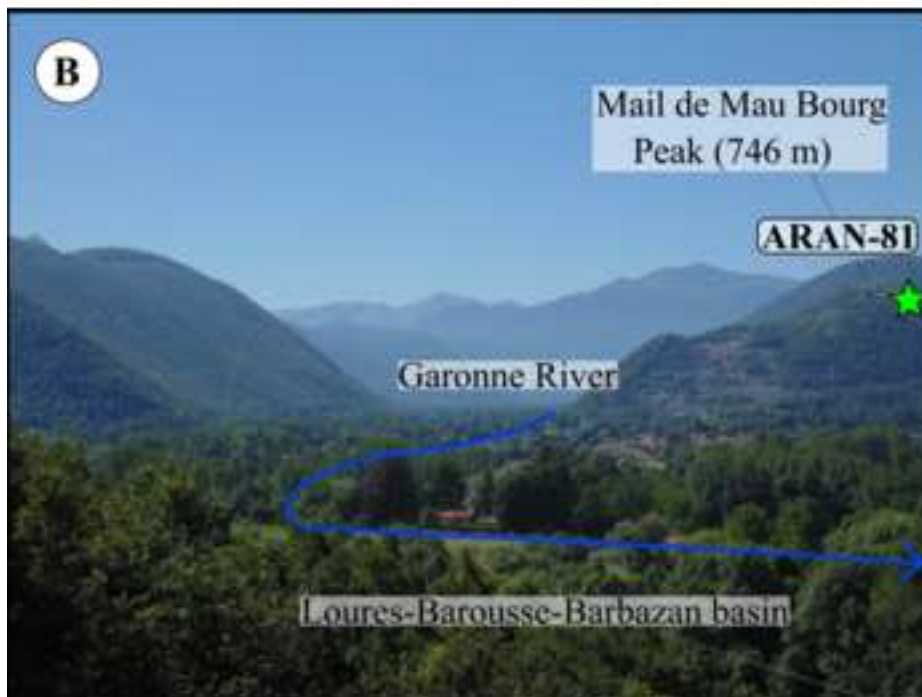
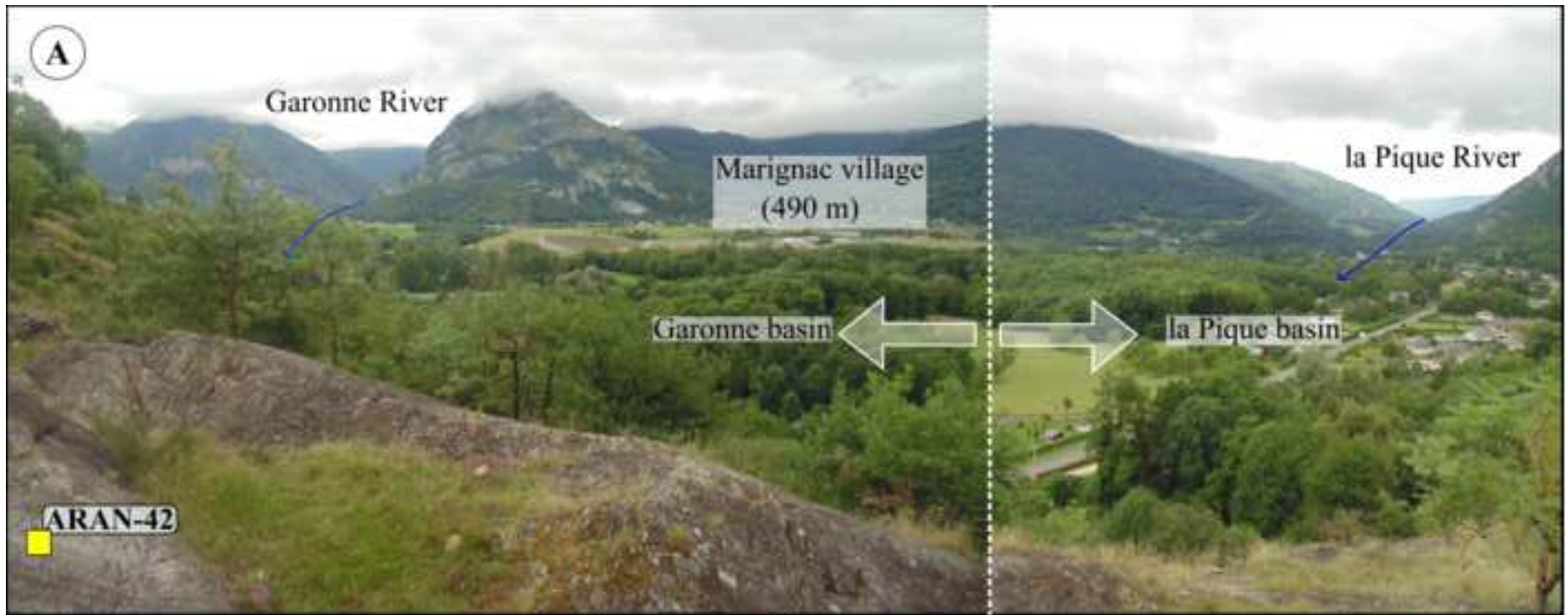
7
8 Figure 4. Moraine complex in the Loures-Barousse-Barbazan basin: (A) Panoramic view of the northernmost
9 part of the basin and moraine ridges of the external moraine system; (B) moraine ridge IM-1 seen from the
10 southernmost part of the basin; (C) moraine ridges IM-2 viewing from the Burs village.

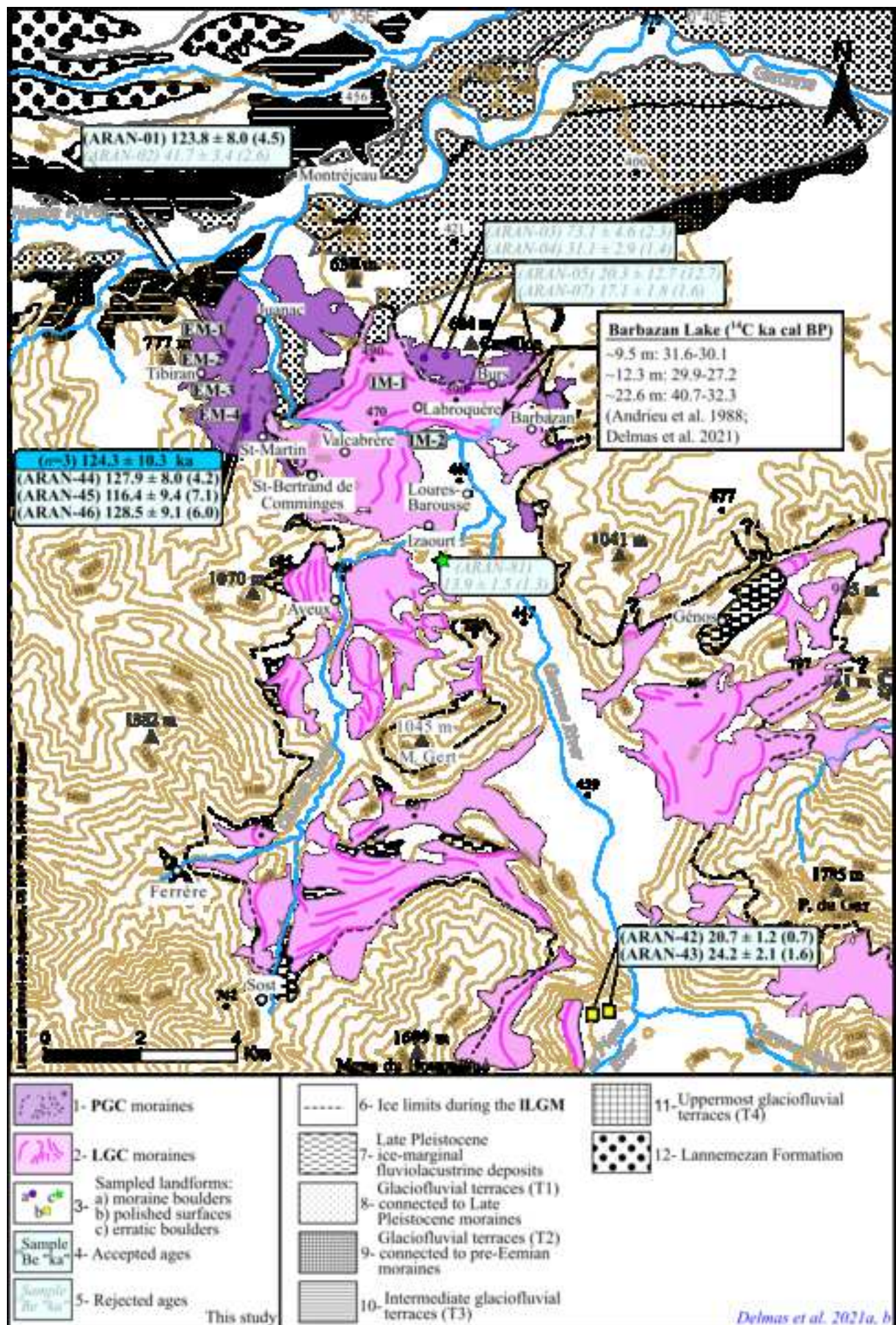
11
12 Figure 5. CRE ages of the different moraine systems from the terminal basin of the Loures-Barousse-Barbazan
13 and polished surfaces upvalley.

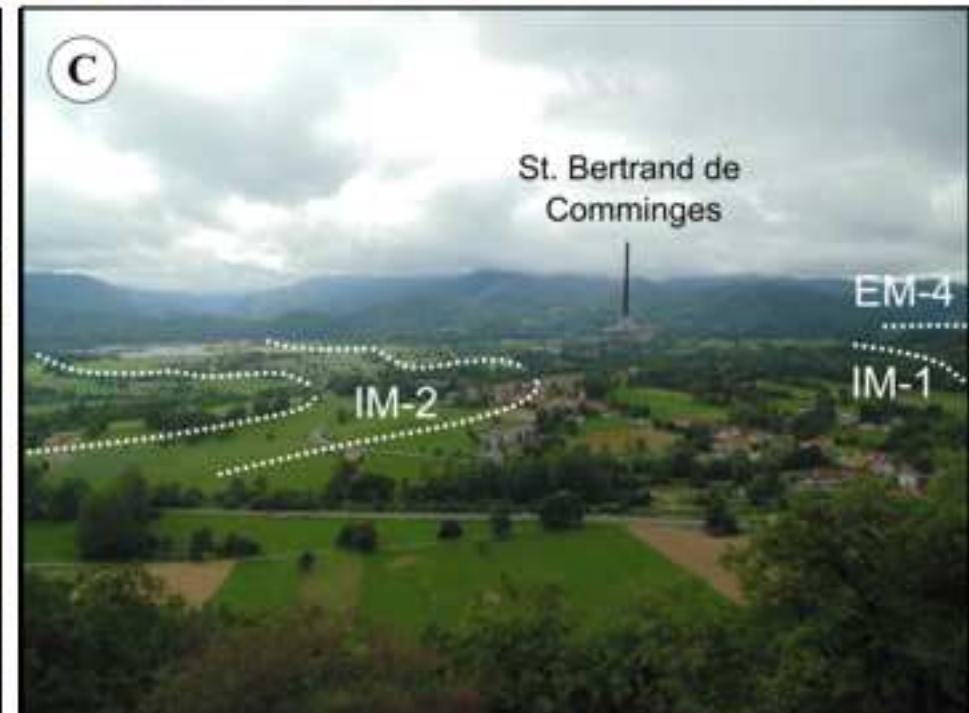
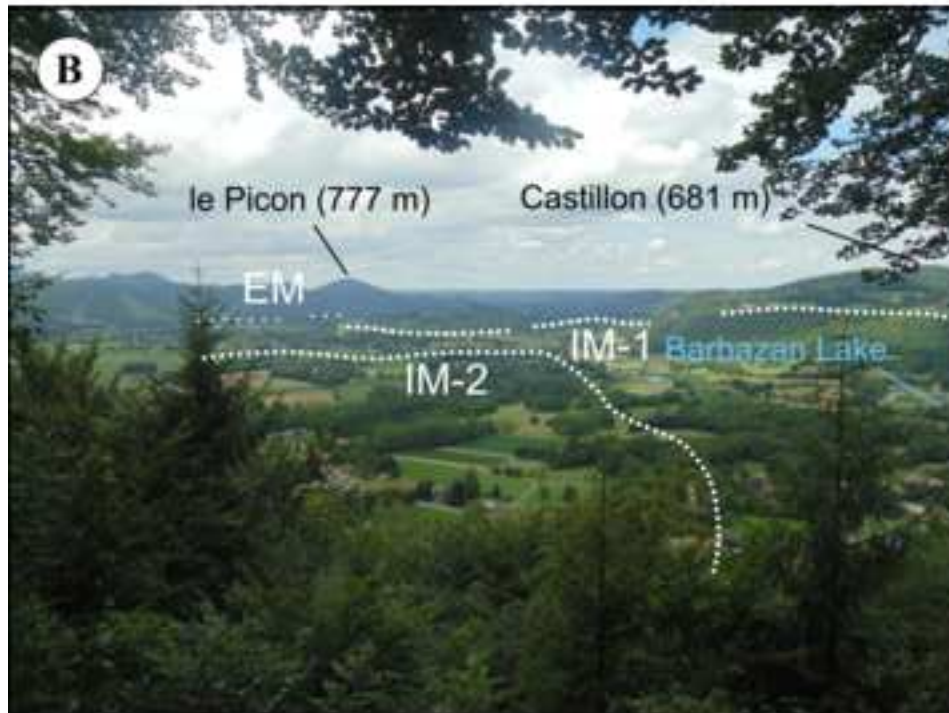
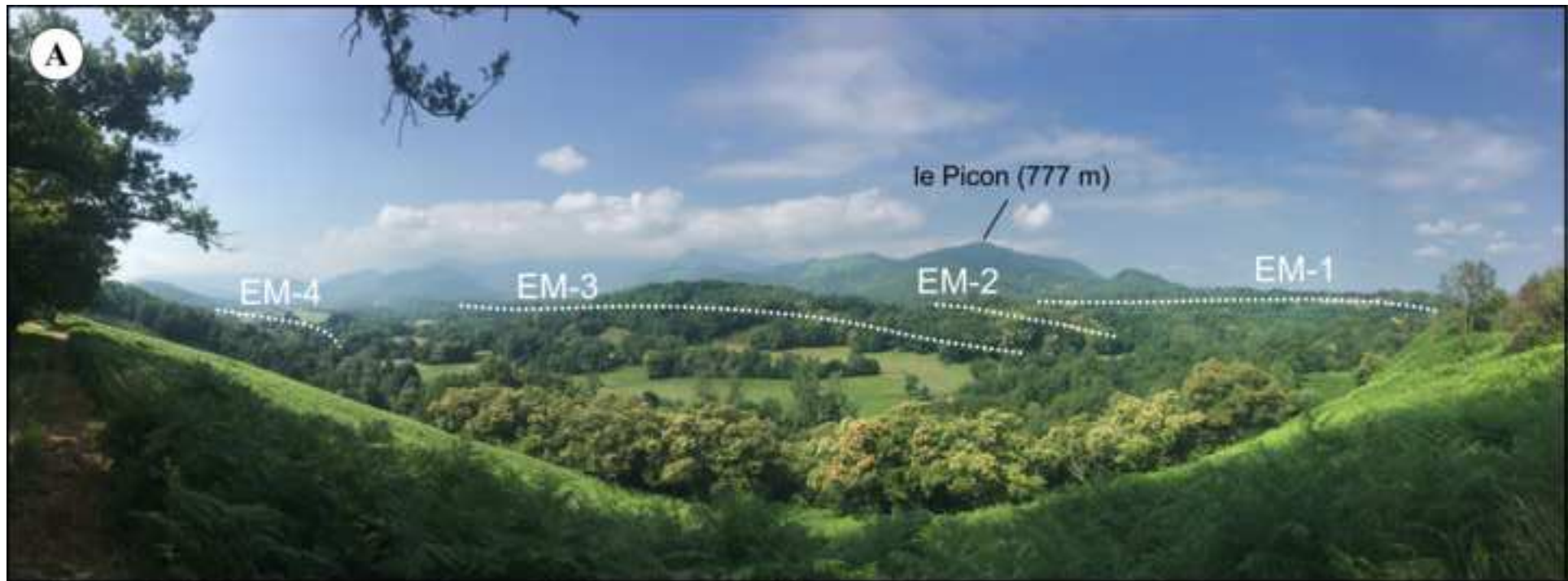
14
15 Figure 6. Terminal position of the Garonne palaeoglacier during the glacial advance of the MIS 6.

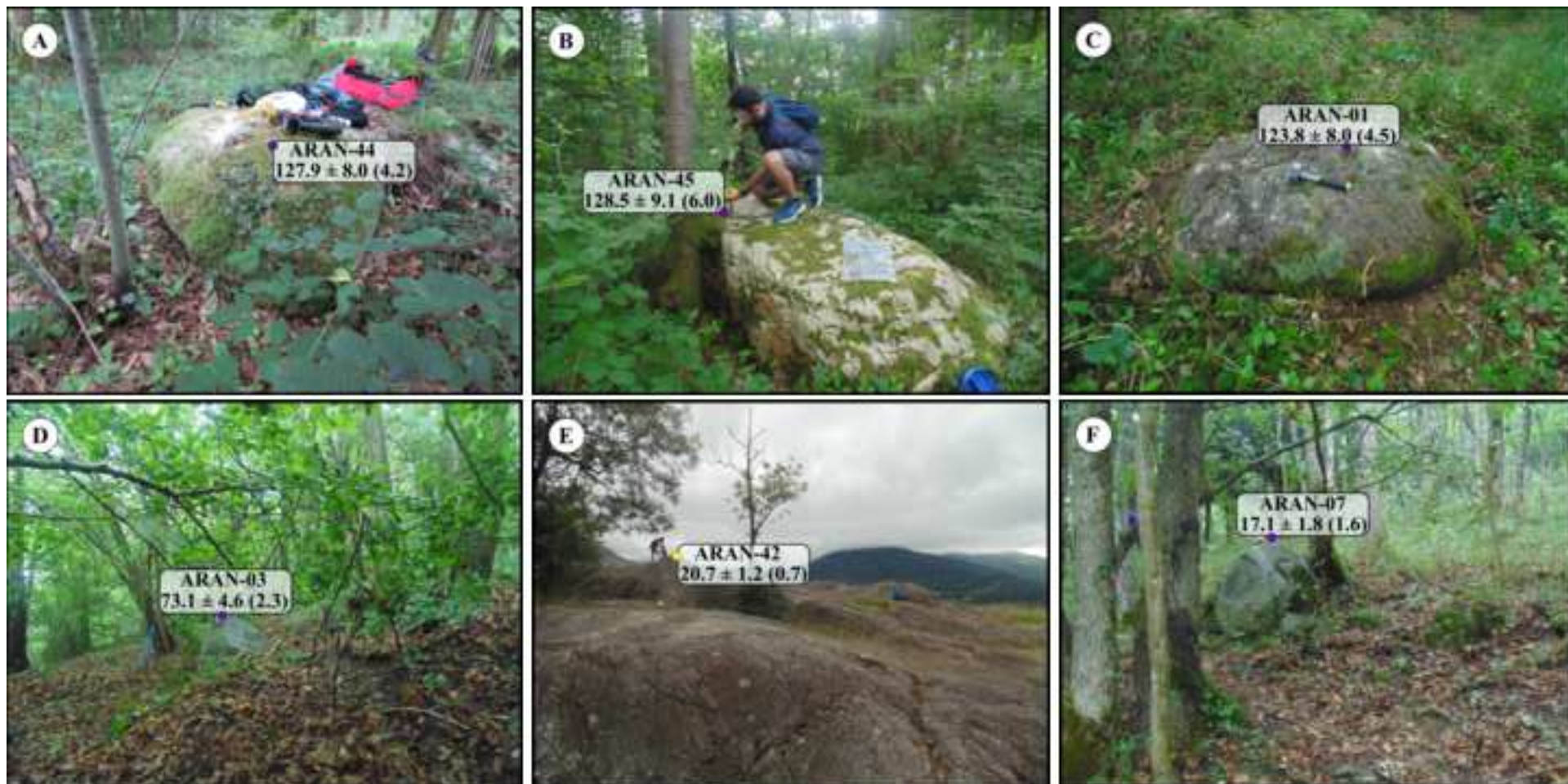
16
17 Figure 7. Normalized probability distribution functions (PDF) of the ^{10}Be CRE exposure ages vs. (A)
18 temperature evolution from the MIS 6 to the gLGM based on the $\delta^{18}\text{O}$ record from the NGRIP ice core from
19 Greenland (time periods are defined after Rasmussen et al. (2014)); percentage of grain size ($>150\ \mu\text{m}$) per
20 sample in ice-rafted debris (IRD) from ocean sediments cores (McManus et al. 1999); benthic $\delta^{18}\text{O}$ record
21 from global distribution (Lisiecki and Raymo 2005); and (B) other CRE dated glacial landforms. The plots of
22 the units result from the sum of the individual PDF of the samples belonging to them. Cold (warm) phases are
23 represented by the blue (red) bands.
24
25
26
27
28
29
30
31
32
33
34
35
36
37
38
39
40
41
42
43
44
45
46
47
48
49
50
51
52
53
54
55
56
57
58
59
60
61
62
63
64
65

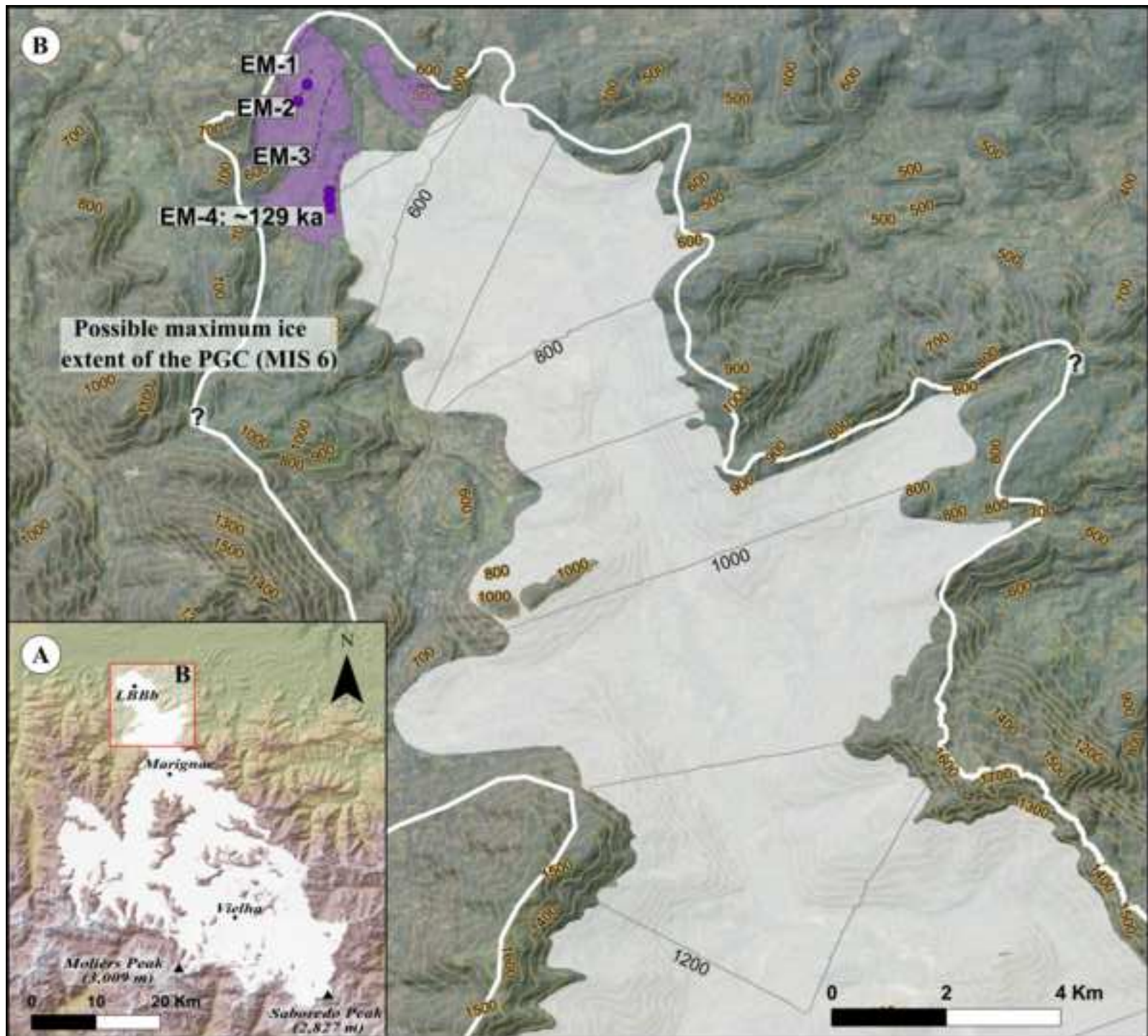












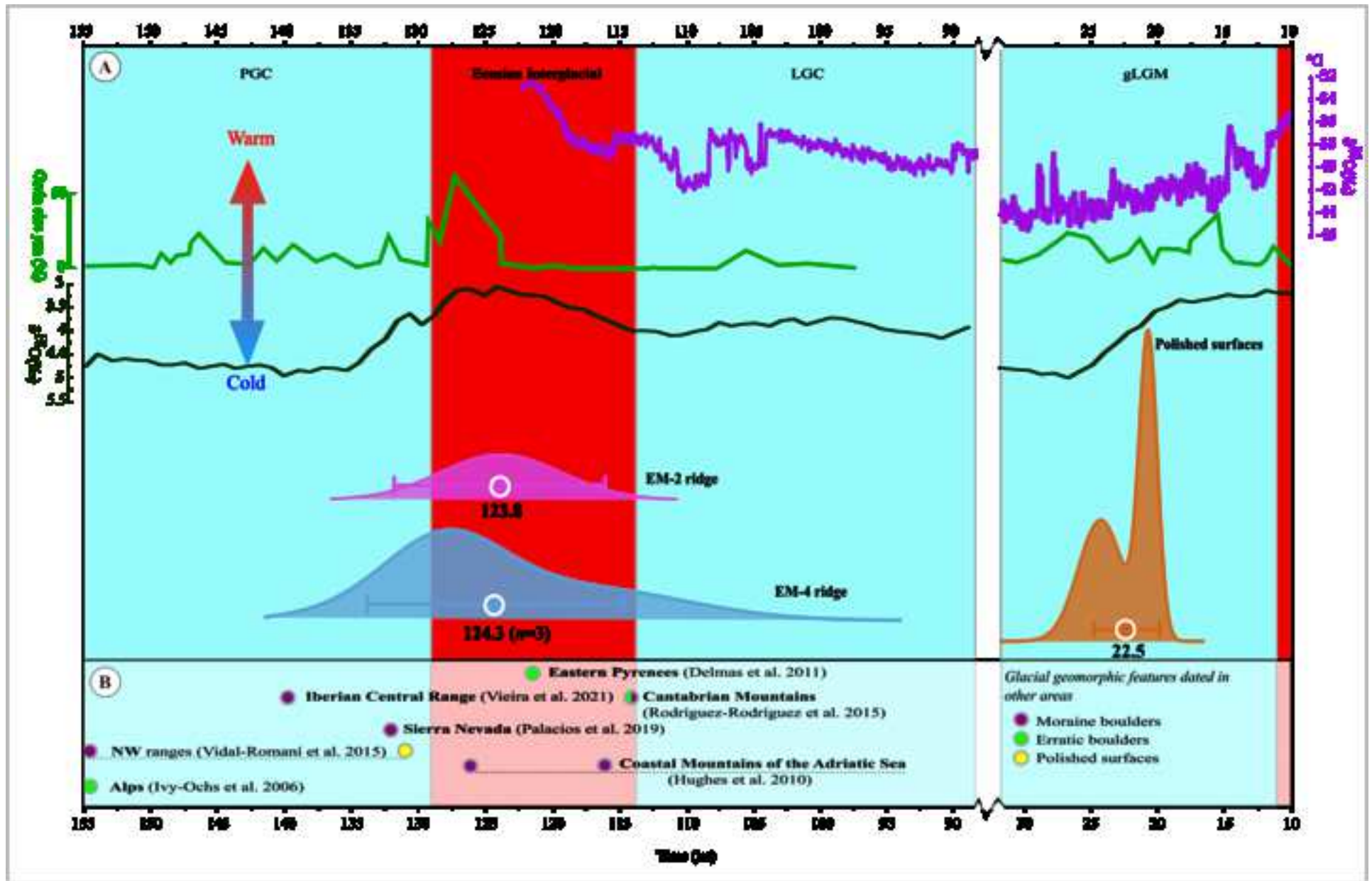


Table 1. Sample and field data.

Sample name	Landform	Latitude (DD)	Longitude (DD)	Elevation (m a.s.l.) ^a	Topographic shielding factor	Thickness (cm)	Lithology
<i>Outermost moraines (EM)</i>							
ARAN-01	(EM-2) Moraine boulder	43.0537	0.5502	477	0.9995	2.0	Quartzite
ARAN-02		43.0538	0.5497	481	0.9995	2.0	Quartzite
ARAN-44	Moraine boulder	43.0388	0.5598	475	0.9871	3.0	Aplite
ARAN-45	(EM-4) Moraine boulder	43.0389	0.5598	475	0.9994	2.8	Quartzite
ARAN-46	Moraine boulder	43.0389	0.5598	474	0.9972	4.5	Quartzite
<i>Highest erratic boulder (EM)</i>							
ARAN-81	Erratic boulder	43.0098	0.6036	680	0.9996	3.0	Granite
<i>Highest moraines of the EM</i>							
ARAN-03	Moraine boulder	43.0466	0.6060	674	1.0000	4.0	Quartzite
ARAN-04	Moraine boulder	43.0473	0.6078	658	0.9966	4.0	Quartzite
<i>Internal moraines (IM)</i>							
ARAN-05	(IM-1) Moraine boulder	43.0425	0.6114	576	0.9989	4.0	Granite
ARAN-07		43.0332	0.6301	590	0.9915	5.0	Granite
<i>Polished surfaces</i>							
ARAN-42	Polished surface	42.9291	0.6454	541	0.9758	4.5	Quartzite
ARAN-43	Polished surface	42.9287	0.6459	525	0.9785	2.5	Quartzite

^a Elevations derived from the 5 m Digital Elevation Model from the Spanish "Instituto Geográfico Nacional" and the French "l'Institut national de l'information géographique et forestière" are subjected to a vertical accuracy of ± 5 m.

Table 2

Table 2. Analytical data and calculated ^{10}Be exposure ages. $^{10}\text{Be}/^9\text{Be}$ ratios were inferred from measurements at the ASTER AMS facility. Individual ages are shown with their full uncertainties (including analytical AMS uncertainty and production rate uncertainty) and analytical uncertainty only within brackets. Arithmetic mean ages are given with their full uncertainties (including standard deviation and production rate uncertainty) and standard deviations only in brackets.

Sample name	Quartz weight (g)	mass of carrier (^9Be mg)	ASTER AMS cathode number	$^{10}\text{Be}/^9\text{Be}$ (10^{-14})	Blank correction (%)	$[^{10}\text{Be}]$ (10^4 atoms g^{-1})	Age (ka)	
<i>External frontal moraines (EM)</i>								
ARAN-01	EM-2	11.41	0.459	CHAU	25.54 \pm 0.96	0.77	68.17 \pm 2.57	123.8 \pm 7.8 (4.5)
ARAN-02		11.66	0.464	CHAV	8.96 \pm 0.59	2.20	23.32 \pm 1.57	<i>41.6 \pm 3.4 (2.6)^a</i>
ARAN-44	EM-4 ($n=3$)	18.70	0.443	IGNJ	43.71 \pm 1.46	0.44	68.85 \pm 2.30	127.9 \pm 8.0 (4.2)
ARAN-45	124.1 \pm 9.6	20.45	0.441	IGNK	44.37 \pm 2.80	0.43	63.63 \pm 4.04	116.4 \pm 9.4 (7.1)
ARAN-46	(5.5) ka	20.76	0.440	IGNL	48.89 \pm 2.29	0.39	68.95 \pm 3.24	128.5 \pm 9.1 (6.0)
<i>Highest erratic boulder (EM)</i>								
ARAN-81		19.23	0.438	IGNU	5.97 \pm 0.57	3.34	8.79 \pm 0.86	<i>13.9 \pm 1.5 (1.3)</i>
<i>Highest moraines of the EM</i>								
ARAN-03		11.19	0.455	CHAW	17.9 \pm 0.55	1.93	47.65 \pm 1.49	<i>73.1 \pm 4.6 (2.3)</i>
ARAN-04		11.61	0.454	CHAX	7.90 \pm 0.34	4.49	19.77 \pm 0.91	<i>31.1 \pm 2.1 (1.4)</i>
<i>Internal moraines</i>								
ARAN-05	IM-1	10.88	0.457	CHAY	4.54 \pm 2.62	8.04	11.78 \pm 7.35	<i>20.3 \pm 12.7 (12.7)</i>
ARAN-07		11.44	0.460	CHAZ	4.01 \pm 0.36	9.10	9.89 \pm 0.96	<i>17.1 \pm 1.8 (1.6)</i>
<i>Polished surfaces</i>								
ARAN-42		21.36	0.432	IGNH	8.58 \pm 0.29	2.33	11.34 \pm 0.39	20.7 \pm 1.2 (0.7)
ARAN-43		18.38	0.436	IGNI	8.67 \pm 0.60	2.29	13.42 \pm 0.95	24.2 \pm 2.1 (1.6)

Chemistry blank details

Blank name	Processed with	mass of carrier (^9Be mg)	ASTER AMS cathode number	$^{10}\text{Be}/^9\text{Be}$ (10^{-14})	$[^{10}\text{Be}]$ (10^4 atoms)		
BK-1	ARAN-3, 4, 5, 7	0.46	CHAT	0.34 \pm 0.04	10.30 \pm 1.24	-	-
BK-3	ARAN-1, 2	0.46	IGHI	0.20 \pm 0.03	5.98 \pm 0.93	-	-
ARAN-BK	ARAN-42, 43, 44, 45, 46, 81	0.43	IGNV	0.20 \pm 0.03	5.65 \pm 0.84	-	-

^a The exposure ages in grey and italics were considered as outliers based on statistical (chi2-test) and geomorphological criteria. Such exposure ages are therefore not included in the interpretation.

Table 3. Exposure ages according to different erosion scenario corrections.

Sample name	Exposure ages (arithmetic mean, in ka)		
	No correction	Erosion correction (0.2 mm/ka)	Erosion correction (1 mm/ka)
<i>Outermost moraines (EM)</i>			
ARAN-1	123.8 ± 7.8 (4.5)	127.1 ± 8.2 (4.7)	143.4 ± 9.7 (5.6)
ARAN-2	<i>41.6 ± 3.4 (2.6)</i>	<i>42.0 ± 3.4 (2.7)</i>	<i>43.4 ± 3.6 (2.8)</i>
ARAN-44	127.9 ± 8.0 (4.2)	131.4 ± 8.3 (4.4)	149.3 ± 9.7 (5.1)
ARAN-45	116.4 ± 9.4 (7.1)	119.3 ± 9.6 (7.3)	133.0 ± 11.1 (8.5)
ARAN-46	128.5 ± 9.1 (6.0)	132.0 ± 9.4 (6.2)	150.1 ± 11.0 (7.2)
<i>mean</i>	<i>124.1 ± 9.6 (5.5)</i>	<i>127.8 ± 11.7 (6.0)</i>	<i>144.1 ± 14.4 (6.9)</i>
<i>Highest moraines</i>			
ARAN-3	<i>73.1 ± 4.6 (2.3)</i>	<i>74.3 ± 4.7 (2.3)</i>	<i>79.3 ± 5.0 (2.5)</i>
ARAN-4	<i>31.1 ± 2.1 (1.4)</i>	<i>31.2 ± 2.1 (1.4)</i>	<i>32.0 ± 2.1 (1.4)</i>
<i>Highest erratic boulder</i>			
ARAN-81	<i>13.9 ± 1.5 (1.3)</i>	<i>14.0 ± 1.5 (1.3)</i>	<i>14.1 ± 1.5 (1.3)</i>
<i>Innermost moraines (IM)</i>			
ARAN-7	<i>17.1 ± 1.8 (1.6)</i>	<i>17.2 ± 1.8 (1.6)</i>	<i>17.4 ± 1.9 (1.6)</i>
<i>Polished surfaces</i>			
ARAN-42	20.7 ± 1.2 (0.7)	20.8 ± 1.2 (0.7)	21.1 ± 1.3 (0.7)
ARAN-43	24.2 ± 2.1 (1.6)	24.3 ± 2.1 (1.6)	24.8 ± 2.1 (1.7)

^a The exposure ages in grey and italics were considered as outliers based on statistical (chi2-test) and geomorphological criteria. Such exposure ages are therefore discarded across the text.

Table 5. Comparison of the glacial chronology of the Penultimate Glaciation in the northern valleys of the Pyrenees.

Range	Valley	Age	Geomorphological unit	Dating Method	Reference
Pyrenees (Northern slope)	Ariège Valley	122 ka	Erratic boulder lying on bedrock	CRE (^{10}Be)	Delmas (2011)
Pyrenees (Southern slope)	Aragón Valley	171 ka	Frontal moraine	OSL	García-Ruiz et al. (2013)
Central Range (Serra da Estrela)	Zêzere Valley	140 ka	Lateral moraine	CRE (^{36}Cl)	Vieira et al. (2021)
Betic Range (Sierra Nevada)	Naute Valley	130-135 ka	Terminal moraine	CRE (^{10}Be)	Palacios et al. (2019)
Cantabrian Mountains	Porma Valley	114 ka	Erratic boulders and ground moraine at the terminal zone	CRE (^{10}Be)	Rodríguez-Rodríguez et al., (2016)
NW ranges (Serra de Queixa-Invernadoiro)	Conso Valley	155 ka	Push moraine boulder	CRE (^{21}Ne)	Vidal-Romaní et al. (2015)
NW ranges (Serra Gerês-Xurés)	Portela da Amoreira divide	131 ka	Polished surface	CRE (^{21}Ne)	Vidal-Romaní et al. (2015)

Table 5. Comparison of the glacial chronology of the Penultimate Glaciation in the northern valleys of the Pyrenees.

Range	Valley	Age	Geomorphological unit	Dating Method	Reference
Pyrenees (Northern slope)	Ariège Valley	122 ka	Erratic boulder lying on bedrock	CRE (^{10}Be)	Delmas (2011)
Pyrenees (Southern slope)	Aragón Valley	171 ka	Frontal moraine	OSL	García-Ruiz et al. (2013)
Central Range (Serra da Estrela)	Zêzere Valley	140 ka	Lateral moraine	CRE (^{36}Cl)	Vieira et al. (2021)
Betic Range (Sierra Nevada)	Naute Valley	130-135 ka	Terminal moraine	CRE (^{10}Be)	Palacios et al. (2019)
Cantabrian Mountains	Porma Valley	114 ka	Erratic boulders and ground moraine at the terminal zone	CRE (^{10}Be)	Rodríguez-Rodríguez et al., (2016)
NW ranges (Serra de Queixa-Invernadoiro)	Conso Valley	155 ka	Push moraine boulder	CRE (^{21}Ne)	Vidal-Romaní et al. (2015)
NW ranges (Serra Gerês-Xurés)	Portela da Amoreira divide	131 ka	Polished surface	CRE (^{21}Ne)	Vidal-Romaní et al. (2015)